Pharmacological Research 201 (2024) 107087

Contents lists available at ScienceDirect

Pharmacological Research

journal homepage: www.elsevier.com/locate/yphrs

The dangerous "West Coast Swing" by hyperglycaemia and chronic stress in the mouse hippocampus: Role of kynurenine catabolism

Micaela Gliozzi [a,*,1], Anna Rita Coppoletta [a,1], Antonio Cardamone [a,1], Vincenzo Musolino [b,*,2], Cristina Carresi [c,2], Saverio Nucera [a], Stefano Ruga [a], Federica Scarano [a], Francesca Bosco [d], Lorenza Guarnieri [d], Roberta Macrì [a], Rocco Mollace [a,e], Catherine Belzung [f,3], Vincenzo Mollace [a,3]

[a] Pharmacology Laboratory, Institute of Research for Food Safety and Health IRC-FSH, Department of Health Sciences, University Magna Græcia of Catanzaro, 88100 Catanzaro, Italy
[b] Laboratory of Pharmaceutical Biology, Department of Health Sciences, Institute of Research for Food Safety & Health IRC-FSH, University "Magna Græcia" of Catanzaro, 88100 Catanzaro, Italy
[c] Veterinary Pharmacology Laboratory, Institute of Research for Food Safety and Health IRC-FSH, Department of Health Sciences, University Magna Graecia of Catanzaro, 88100 Catanzaro, Italy
[d] Department of Health Sciences, University Magna Graecia of Catanzaro, 88100 Catanzaro, Italy
[e] Department of Systems Medicine, University of Rome Tor Vergata, Italy
[f] UMR 1253, iBrain, Inserm, Université de Tours, CEDEX 1, 37032 Tours, France

ARTICLE INFO

Keywords:
Hyperglycaemia
Unpredictable chronic mild stress (UCMS)
Kynurenine
Quinolinic acid and neurodegeneration
Glutamatergic synapse and apoptosis
Diabetes
And depression

ABSTRACT

Growing epidemiological studies highlight a bi-directional relationship between depressive symptoms and diabetes mellitus. However, the detrimental impact of their co-existence on mental health suggests the need to treat this comorbidity as a separate entity rather than the two different pathologies. Herein, we characterized the peculiar mechanisms activated in mouse hippocampus from the concurrent development of hyperglycaemia, characterizing the different diabetes subtypes, and chronic stress, recognized as a possible factor predisposing to major depression. Our work demonstrates that kynurenine overproduction, leading to apoptosis in the hippocampus, is triggered in a different way depending on hyperglycaemia or chronic stress. Indeed, in the former, kynurenine appears produced by infiltered macrophages whereas, in the latter, peripheral kynurenine preferentially promotes resident microglia activation. In this scenario, QA, derived from kynurenine catabolism, appears a key mediator causing glutamatergic synapse dysfunction and apoptosis, thus contributing to brain atrophy. We demonstrated that the coexistence of hyperglycaemia and chronic stress worsened hippocampal damage through alternative mechanisms, such as GLUT-4 and BDNF down-expression, denoting mitochondrial dysfunction and apoptosis on one hand and evoking the compromission of neurogenesis on the other. Overall, in the degeneration of neurovascular unit, hyperglycaemia and chronic stress interacted each other as the partners of a "West Coast Swing" in which the leading role can be assumed alternatively by each partner of the dance. The comprehension of these mechanisms can open novel perspectives in the management of diabetic/depressed patients, but also in the understanding the pathogenesis of other neurodegenerative disease characterized by the compromission of hippocampal function.

1. Introduction

Diabetic patients show high frequency of depressive symptoms with a negative effect on disease outcomes. On the other hand, subjects suffering from depression manifested an increased risk of a wide range of chronic disease, including obesity and diabetes, that result in a

* Corresponding authors.
E-mail addresses: gliozzi@unicz.it (M. Gliozzi), v.musolino@unicz.it (V. Musolino).
[1] First authors equally contribution
[2] Second authors equally contribution
[3] Last authors equally contribution

https://doi.org/10.1016/j.phrs.2024.107087
Received 27 September 2023; Received in revised form 25 January 2024; Accepted 26 January 2024
Available online 30 January 2024

worsening of the quality of life and an increase of premature death [1–7].

The etiopathogenesis of the two pathologies can share common aspects and, among them, stressful or traumatic events, can cause similar clinical signs, such as behavioural alterations and mood disorders, that typified diabetic as well as depressed subjects [8–12]. At biological level, the bidirectionality underlying the relationship between diabetes and depression can depend on several mechanisms, such as innate inflammatory response, the hypothalamic-pituitary-adrenal (HPA) axis, and insulin resistance, able to reciprocally interact [8,13,14]. In this scenario, a growing attention is paid toward a specific approach aimed to manage diabetes and comorbid depressive symptoms [15].

Persistent hyperglycaemia is the main characteristic unifying type 1 and type 2 diabetes [8] and, independently from their different pathogenesis, growing literature supports the hypothesis of a connection between hyperglycaemia and neuroinflammation [15].

Chronic hyperglycaemia can cause a constant low-grade inflammation and can also induce kynurenine pathway (KP), both responsible for the alteration of brain functions [16]. Furthermore, several neuropsychiatric disorders are characterized by the overactivation of KP [17–20] and the development of brain inflammation [21], leading to mood and cognition disorders [22]. Among them, major depression is associated with the reduction of hippocampal volume or of its specific subregions, such as the Dentate Gyrus (DG) or the CA1 and CA3 regions [23,24]. Coherently, the altered functions characterizing patient suffering from major depression concern information encoding and processing, episodic memory, emotions, and regulation of stress hormones [25].

The main branches of KP are segregated in the brain and depend on cell type. Kynurenic acid (KA) branch is preferentially localized in astrocytes, whereas the NAD^+ branch operates primarily in microglia [26]. This specific localization in the resident microglia indicates that KP activity relates to neuroinflammation, typical of several central nervous system diseases [27].

Among the KP intermediates, Quinolinic Acid (QA) can act in a dual mode: classical metabolite and/or potent neurotoxin [28]. As metabolite, it participates in the *de novo* synthesis of NAD^+, synthesized to maintain energy production in response to inflammatory processes and to oxidative and metabolic stresses [28], whereas, as neurotoxin, it promotes the pathogenesis of different neurological diseases [29]. The neurotoxic effect could be mediated by its selective binding to *N*-methyl-*D*-aspartate (NMDA) receptors that favours calcium entry into neurons and astrocytes. Moreover, excitotoxic injury especially involves neurons expressing NR2A and NR2B (which are subtypes of NMDA receptors) in the hippocampus and in the striatum [30–36].

Moreover, QA can influence intracellular energetic balance, impairing cellular respiration and ATP synthesis [37,38], and can alter the activity of intracellular antioxidant systems [39–41] leading to mitochondrial dysfunction, free radical overproduction and, finally, to apoptotic cell death [42–44].

Although, the impact of KP dysregulation on hippocampal neuroinflammation under hyperglycaemia and chronic stress, singularly, has been partially clarified, to date, the molecular mechanisms underlying the detrimental effects caused by their interaction are not still investigated. In this consideration, the aim of the present work was to study the role of KP in the development of inflammatory damage induced by their association, to discover novel pharmacological targets aimed to counteract neuroinflammatory mechanisms that might be implicated also in other neurodegenerative disease.

2. Materials and methods

2.1. Animals

C57BL/6 male mice: 26.44 ± 0.29 g, 8 weeks old were purchased from Envigo RMS Srl (Udine, Italy) and housed under standard laboratory conditions in a specific-pathogen-free animal facility and maintained at 22 ± 2 °C and 55% ± 5% humidity, with a 12-h light-dark cycle and free access to food (standard rodent chow diet, Teklad™, Envigo) and water. All the experimental procedures were performed according to the protocols approved by the Animal Care of University Magna Graecia of Catanzaro (n. 957/2017-PR), in accordance with the European Commission guidelines (Directive 2010/63/EU) for the animals used for scientific purposes.

2.2. Study design

Before starting the experiment, mice were randomly assigned to 4 groups (n = 10 animals/group): control (CTRL), unpredictable chronic mild stress (UCMS), high blood glucose (HBG), unpredictable mild stress + high blood glucose (UCMS+HBG) (Fig. 1). Body weight and body composition were registered weekly until the end of the study. An a priori power analysis was conducted using G*Power (v 3.1.9.6) to establish the sample size of the study [45]. Results highlighted that the required sample size to reach an 80% power for detecting a medium effect, at a significance level of $\alpha = .05$, was $N = 40$ (10 each group) for one-way ANOVA.

Starting from day 1, multiple, low doses of streptozotocin (STZ) (Sigma Aldrich, #S0130, Milan, Italy) (40 mg/kg, intraperitoneally, i.p.) were injected to mice on 5 consecutive days in HBG and UCMS+HBG groups (Fig. 1), using 1-ml syringes and 25-G needles. STZ was dissolved in 50 mM sodium citrate (Sigma Aldrich, #61312–04-3, Milan, Italy) buffer (pH 4.5) to a final concentration of 4 mg/ml, 5 min prior the administration. Four hours before the injection, the food was removed from all cages whereas water was provided normally. After 9 days from the last STZ injection, blood glucose levels from a tail-vein blood sample were analysed in fasted mice using a glucometer (MultiCare In, Biochemical Systems International, Arezzo, Italy), to ensure the occurrence of hyperglycaemia in the STZ-treated animals.

On day 15, animals (UCMS and UCMS+HBG groups) were individually housed and exposed to UCMS protocol which lasted 7 weeks (Fig. 1). Specifically, mice were exposed to daily mild psychosocial stressors, in an unpredictable manner, to avoid any habituation of the animals, between 10:00 and 18:00, to cause physical, behavioural, biochemical, and physiological alterations. The following experimental stressors were applied: social stress, cage change, rat faeces, water stress, restraint stress, sawdust change, cycle disturbances. The characteristics and the schedule of the stressors were carried out according to the protocol of Nollet et al. [46].

Physical changes were quantified by measuring the coat state and body weight of the animals. Other signs of stress (i.e., anxiety- and depressive-like behaviours) were assessed performing the following behavioural tests: the nest building test, the open field test, and the tail suspension test (Fig. 1). At the end of the experiment the animals were anesthetized with 5% isoflurane and euthanized (Fig. 1). The brain was excised and sectioned to dissect hippocampal area. In addition, all the organs were weighed, sectioned, and fixed in formalin or frozen in liquid nitrogen for further analysis.

2.3. Body composition analysis

Total body fat, lean mass, and body fluids were assessed through nuclear magnetic resonance spectroscopy (EchoMRI-700, Echo Medical Systems, Houston, TX, USA), as previously described [47].

2.4. Coat state

The coat state was examined using a data-masking approach. The deterioration of the coat state, related to a disturbance of self-directed behaviour (decrease of grooming), was mainly evaluated on the head, the neck, and the back of mice, as well as on the abdomen and the hind paws. Finally, a complete assessment of the coat state was carried out. Each zone was scored as follow: a) 0 good state (smooth and shiny fur,

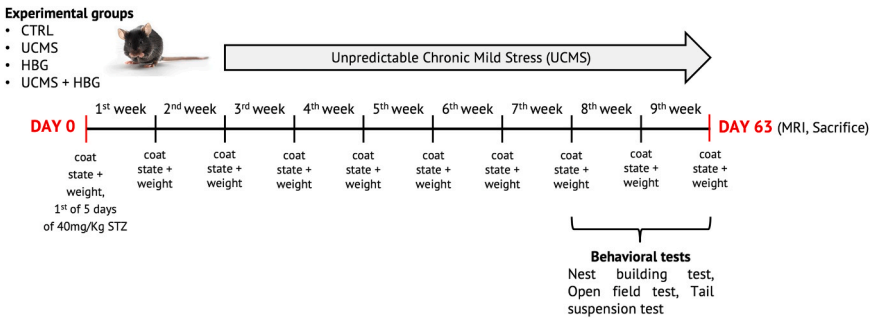

Fig. 1. Study Design.

with no tousled, spiky patches); b) 0.5 moderately bad state (slightly fluffy fur with some spiky patches); c) 1 bad state (dirty and fluffy fur on most of the body with slight staining). The maximum global score didn't exceed.

2.5. Nest building test

Non-UCMS mice (CTRL and HBG groups) were isolated in individual cages for 24 h before the starting of the test, whereas stressed animals (UCMS and UCMS+HBG) were already individually housed. A cotton nestlet was placed in each cage one hour before the dark phase (active phase). At 5 and 23 h after the beginning of the dark phase, the nest quality was evaluated using the following parameters: a) Score 1: intact cotton square; b) Score 2: partially used cotton square; c) Score 3: scattered cotton without any form of nest; d) Score 4: gathered cotton with a "flat nest"; e) Score 5: gathered cotton in form of a "ball" with a small passage for entry of the mouse, like an igloo, with or without roof.

2.6. Open field test (OFT)

The open field was a squared arena surrounded by a wall. The field was divided into 9 squares. The four central squares corresponded to the "centre" of the field. The mouse was placed in the centre of the field, and, during the test, the time spent in the centre and the number of centre entries were analysed. The total covered distance was also calculated for each animal over a 5-minute period, using EthoVision software (Program 3.1, Noldus, The Netherlands) [48].

2.7. Tail suspension test (TST)

Tail suspension test (TST) was performed using experimental procedure frequently described by others. Mice were placed in a tail suspension test apparatus (Bioseb, USA/Canada), made of white acrylic walls (20 × 40 × 60 cm), with one open wall for video recording. Each mouse was suspended by the tail and the resultant behaviour was recorded by a video camera for 5 min. The principle is based on the quantity of movement generated by a mouse trying to escape from its suspension. During the test, the movements are analysed in terms of time of immobility and energy developed over time. The energy parameter represents the amount of kinetic energy exhibited by the animal during the test. It reflects the overall motor activity and movement, providing insights into the animal's response to the stress of being suspended. The energy is a unique way to differentiate between passive swinging and active struggling. These two parameters were calculated using the Bioseb Tail Suspension Test software (Bioseb in vivo research instruments, Pinellas Park, USA).

2.8. ^{1}H-MRS

Animals were anaesthetized with 4% of isoflurane (Forane Abott) vaporized in O_2 (flow: 2 l/min) and anaesthesia was kept between 1.5% and 2% to maintain the breathing rhythm (SA Instruments, Inc., Stony Brook, NY, USA) between 50 and 80 breaths per minute during the MRI acquisition; the body temperature was monitored and maintained at 37 °C (SA Instruments, Inc., Stony Brook, NY, USA).

^{1}H-MRS spectra were acquired with a Bruker Pharmascan 70/16 US 7 T bore MR scanner (Bruker Biospin MRI GmbH, Ettlingen, Germany), equipped with a Bruker's MRI CryoProbe™ with MRI cryocooler, as previously described [49].

Following a three-axis localizer scan and Axial and Sagittal T2_turboRARE weighted images with fat suppression acquisition (35.00 ms echo time, 2500.00 ms repetition time, 2 averages, 9 slices of 0.7 mm thickness each, 20 × 20 mm field of view, 256 × 256 image size), voxel was accurately placed in the hippocampus (2 ×1 x 2 mm^3 voxel size).

Variable power radiofrequency pulses with optimized relaxation delays (VAPOR) water-suppression module was used prior to acquire water suppressed spectra and the VAPOR pulses and delays timing were manually optimized to reduce residual water signal.

Then, PRESS_1H sequence (16.6 ms echo time, 8.99 ms echo time 1, 7.61 ms echo time 2, 2500 ms repetition time, 256 averages, 2 dummy scans, VOI 2 x 1 x 2 mm) was performed.

The absolute quantification of hippocampal metabolites concentrations were performed by TARQUIN software (v. 4.3.10), using the water suppressed spectra data file ("fid") and the water unsuppressed spectra data file ("fid.refscan") provided by the ^{1}H-MRS acquisition.

2.9. Volumetric analysis

Total cerebral brain volumes (TCBVs) analysis was performed using OsiriX imaging software (v. 12.5.3, Pixmeo SARL, Switzerland), as previously described (https://doi.org/10.1038/s41598–022-05228–5). T1_FLASH_3D_iso coronal images with fat suppression of 112.78 μm thick each (8 ms echo time, 50 ms repetition time, 1 average, 20 dummy scans, 133 x 133 x 80 image size, 15 × 15 × 10 mm field of view) were used.

Starting from the olfactory bulbs up to the last part of the cerebellum, ROIs were traced, followed by "Generate Missing ROIs" function. Finally, "Compute ROI Volume" tool was used to merge the ROIs of the entire brain and estimate its volume.

2.10. Serum glucose quantification

Blood was collected via cardiac puncture from the heart of euthanized mice. A volume of around 600 μl of whole blood was centrifuged for 15 min at 1500 g at 4 °C. The serum was collected and immediately analysed for glucose quantification. Glucose (GLU) was measured, using an automatic chemistry analyser, XL-640 (Erba Mannheim) and the Erba liquid stable reagents: glucose (GLU 440, XSYS0012). A serum aliquot was collected and stored at − 80 °C for further immunoassays.

2.11. Measurement of serum VEGF level

The concentrations of serum VEGF were measured through ProcartaPlex Multiplex Immunoassay Kit (PPX-15, assay ID: MX9HJZD, Thermo Fisher Scientific, Milan, Italy), according to the manufacturer's instructions, at Thermo Fisher Scientific Bender MedSystems GmbH (Campus Vienna Biocenter, Vienna, Austria).

2.12. Enzyme-linked immunosorbent assay (ELISA) for L-kynurenine/tryptophan ratio determination

L-kynurenine and tryptophan concentrations in the serum were measured using a commercial ELISA kit according to the manufacturer's instructions (ISE-2227, ImmuSmol, Inc., France). Briefly, after acylation, L-kynurenine was quantitatively determined by ELISA, whereas the quantification of tryptophan was carried out after its derivatization. Acylated-L-kynurenine and derivatized tryptophan were then incubated overnight to carry out the reaction of competition with solid-phase-bound antigens. The reaction was detected revealing the colour development derived from 3,3′,5,5′-tetramethylbenzidine oxidation. The colorimetric reaction, catalysed from the anti-rabbit IgG-conjugate peroxidase, was read at the wavelength of 450 nm using the Thermo Scientific™ Multiskan™ GO Microplate spectrophotometer (Thermo Fisher Scientific Inc., Milano, Italy). L-kynurenine and tryptophan for each sample were quantified interpolating their absorbance with a curve generated from standards supplied by the manufacturer. The range for L-kynurenine measurement was 0.5 μmol/L-50 μmol/L. The range for tryptophan measurement was 15 μmol/L- 150 μmol/L. The L-Kynurenine (μmol/L)/Tryptophan (μmol/L) ratio was calculated.

2.13. Immunofluorescence

Formalin-fixed, paraffin-embedded Section (5 μm thick) were deparaffinized through exposure to xylene and graded alcohols and then washed in water. The slides were heated at 98 °C for 30 min in 10 mM sodium citrate buffer with pH = 6.0 to recover the epitopes. Sections were washed 3 times with phosphate-buffered saline (PBS) 1X and then permeabilized with a PBS 1X/gelatin (0.2% w/v)/Triton (0.25% v/v) solution, twice for 10 min. Afterwards, slides were blocked in a 5% of bovine serum albumin (BSA) (Sigma Aldrich, #A7906, Milan, Italy) blocking solution for 1 h at RT and then incubated overnight at 4 °C in a humidified environment with the 1% Bovine Serum Albumin (BSA) diluted primary antibodies: anti-Ionized calcium-binding adapter molecule 1 (IBA1) antibody, a microglial and macrophage-specific calcium-binding protein, #ab178846, Abcam, Cambridge, UK, 1:300; anti-Transmembrane Protein 119 (TMEM119) antibody, a transmembrane protein that has been reported to be a highly specific microglia marker which has the advantage of distinguishing microglia from macrophages, #ab209064, Abcam, Cambridge, UK, 1:200; anti-Glial fibrillary acidic protein (GFAP) antibody, that is the intermediate filament expressed in astrocytes, G3893, Sigma Aldrich, Milan, Italy, 1:200; anti-β III Tubulin (TUBB3) antibody which is widely used as a neuron- specific marker, #MAB1637, Sigma Aldrich, Milan, Italy, 1:250; anti-L-kynurenine (KYN) antibody, which is a product of tryptophan metabolism, #IS003, Immusmol, Bordeaux, France, 1:100; anti-Acid Quinolinic (QUIN) antibody, a neurotoxic metabolite of kynurenine, #IS002, Immusmol, Bordeaux, France, 1:100. After the incubation period, each slide was washed three times with PBS 1X and, after a permeabilization step, incubated with a fluorescent secondary antibody Alexa Fluor 488 (green), #A11029; Alexa Fluor 594 (red), Alexa Fluor 555 (green), #A31570; Alexa Fluor 594 (red), #A21207, Thermo Fisher Scientific, Italy) for 1 h at RT. Then, nuclei were stained with DAPI (0.1 μg/ml, #D8417, Sigma Aldrich, Milan, Italy) for 10 min at RT.

2.14. Terminal deoxynucleotidyl transferase dUTP Nick end Labeling (TUNEL) assay

The DeadEnd™ Fluorometric TUNEL System, (#G3250, Promega, USA), is considered as a gold standard of cells apoptosis quantification. This system measures nuclear DNA fragmentation, that is an important biochemical marker of apoptosis. The kit measures the fragmented DNA of apoptotic cells by catalytically incorporating fluorescein-12-dUTP at 3´-OH DNA ends employing Terminal Deoxynucleotidyl Transferase (TdT), which forms a polymeric tail. The slices are rehydrated as above described, then, the tissues were fixed by dipping them in paraformaldehyde. The slices were coated with Proteinase K (provided by the kit), incubated at 37 °C for 10 min and washed with PBS.

The TUNEL reaction solution was added to the slices, and they were incubated at 37 °C in the dark for 60 min in a humidified chamber to allow the reaction. Stain the samples by immersing the slides in 40 ml of propidium iodide, (#J66764. MC, Thermo Scientific, Massachusetts, USA), diluted 1 μg/ml in PBS, for 15 min at room temperature, in the dark. Afterwards, the slices were washed in H_2Odd, dried, and whipped. Finally, DNA labelled with fluorescein-12-dUTP by fluorescence microscopy has been directly observed.

2.15. Immunofluorescence-derived image analysis

Fluorescence was detected using a confocal laser scanning microscope TCS SP5 (Leica Microsystems, Wetzlar, Germany) and a 63X objective was used to acquire confocal images. Images acquired were analysed using ImageJ Fiji (version 2.3.0/1.53 f, NIH, Bethesda, MD, USA). The minimum threshold value (80–255 IBA1; 70–255 TMEM119; 75–255 GFAP; 75–255 KYN; 75–255 QUIN; 95–255 TUBB3) was picked and kept constant between matching hippocampal regions of each mice cohort. Skeleton analysis, allowing microglia and astrocyte ramification evaluation and analysis within entire photomicrographs, was performed using IBA1 positive images for all microglia processes, GFAP positive images for all astrocyte processes, whereas TUBB3 positive images were used as neuron-specific marker. Firstly, single-pixel background fluorescence was erased by noise despeckle tool, then, following resulting images binary conversion, "Skeletonize" tool was performed. This analysis technique provides information regarding microglia, astrocyte, and neuron morphology. Moreover, the neuronal network alterations were analysed performing a neurons total area measurement (Soma + neurite) in TUBB3 positive images.

QUIN-IBA1 and KYN-TMEM119 colocalizations were assessed using colour threshold plugin (default thresholding method, B&W threshold colour, RGB colour space, and dark background).

ImageJ Fiji automated multichannel thresholding (90–255 for both red and green channels) was performed to identify colocalized TUNEL+ pixels as cell apoptosis measurement. Finally, "Analyze particles" tool was carried out to quantitate TUNEL+ fragments.

2.16. Protein extraction and western blotting

Protein extraction was carried out using the AllPrep DNA/RNA/Protein (#80004, QIAGEN, Germany). This kit allows the purification of genomic DNA, total RNA, and total proteins from the same tissue sample, simultaneously.

20 μl of the supernatant was used for total protein concentration through Pierce™ BCA Protein Assay Kit (#23225, Thermo Scientific, Massachusetts, USA) using bovine serum albumin, (Quick Start Bovine Serum Albumin Standard, #500–0206, Bio-Rad, Hercules, USA) as a standard. The proteins were denatured for 5 min at 95 °C in sample loading buffer (500 mM Tris/HCl, pH 6.8; 30% glycerol; 10% sodium dodecyl sulfate; 5% β-mercaptoethanol; and 0.024% bromophenol blue) and 10 μg protein lysate were resolved by sodium dodecyl sulphate polyacrylamide gel electrophoresis. The nitrocellulose membrane (Amersham Protan 0.2 μm NC #10600001, Little Chalfont, UK) were

blocked with Tris / HCl (pH 7.6) containing 0.1% Tween 20% and 5% BSA or 5% milk (Skim Milk Powder, #42590.02, Serva serving scientists, Heidelberg, Germany) for 1 h and incubated overnight at 4 °C shaking, with the following primaries antibodies: anti- OPA1 (Cell Signaling #80471, Danvers, MA, USA); anti- BDNF (Novus Biologicals, NBP2–67410); anti- VDAC1 (Abcam ab34726, Cambridge, United Kingdom); anti-MnSOD (Stressgen biotechnolgies, #SOD111, California, USA); anti-phospho DRP1 (Cell Signaling #4867 s, Danvers, MA, USA); anti GLUT-4 (Abcam ab48547, Cambridge, United Kingdom); anti-NMDA2R (Abcam #ab124913, Cambridge, United Kingdom); anti-NADPH Oxidase-4 (Abcam #ab109225, Cambridge, United Kingdom); anti-Glutamine Synthetase (Abcam #ab176562, Cambridge, United Kingdom); anti- neuronal nitric oxide (NO) synthase (nNOS) (BD Biosciences #611852, Franklin Lakes, New Jersey, USA). The membranes were then washed in Tris-buffered saline (TBS, pH 7.6) with 0.1% Tween-20 and incubated with horseradish peroxidase-conjugated secondary antibodies (Pierce anti-rabbit antibody #31460 or Pierce anti-mouse antibody #31430, Invitrogen, Carlsbad, CA, USA) for 1 h at room temperature. The bound antibody was visualized using a chemiluminescent kit (ECL WB Detection, GE Healthcare RPN210601819, Little Chalfont, UK). The immunoblot scan was performed through the UVITEC program (UVITEC Imaging Systems, Cambridge, United Kingdom), while the analysis was performed through ImageJ Fiji (version 2.3.0/1.53 f, NIH, Bethesda, MD, USA).

2.17. Statistical analysis

Data were analysed with GraphPad PRISM 9.3.1 (GraphPad Software, Inc., La Jolla, CA, USA). The results were expressed as mean ± S.E.M. (Standard Error of the Mean). Normality was tested using Shapiro–Wilk normality test. Normally distributed data were analysed by one way ANOVA followed by Tukey's test, while data without normal distribution were analysed using Kruskal–Wallis analysis of variance followed by Dunn's tests. A repeated measures ANOVA was performed to compare the effect of single or both pathological conditions on the deterioration of the coat state overtime. The sphericity assumption was checked by Mauchly's test, then, a Greenhouse-Geisser correction was performed to adjust the violation of the sphericity assumption. Tukey's post hoc test was performed for pairwise comparisons. P-values < 0.05 were considered statistically significant. The effect of the kynurenine and glucose serum levels to the TCBVs reduction was analysed by multiple regression. Correlation analysis was assessed using Pearson's correlation coefficient.

3. Results

3.1. Chronic stress, hyperglycaemia and the association of both conditions impair body weight, body composition and affect coat state deterioration

Baseline body weight, lean and fat mass were similar in all the randomized groups at the time 0. Before starting behavioural tests (week 7), UCMS and HBG groups significantly lost body weight, though weight loss was significantly marked in HBG mice (Fig. 2A). Interestingly, the weight loss was significantly marked in HBG at week 9 (−15.79%, $p < 0.001$), whereas a gain body weight was observed in UCMS at the end of the experiment (week 9, +5.72%; Fig. 2A). The association with both the pathological conditions exacerbated body weight loss at week 7 (−20.59%, $p < 0.001$; Fig. 2A) and week 9 (−17.21%, $p < 0.001$, Fig. 2A). The alteration of body lean mass showed a similar trend of the body weight (Fig. 2B). Differently, fat mass showed a significant reduction at week 7 in UCMS (−13.57%, $p < 0.01$), HBG (−52.08%, $p < 0.001$) and UCMS+HBG (−58.02%, $p < 0.001$) groups, as well as at week 9 in HBG (−42.98%, $p < 0.001$) and UCMS+HBG (−44.06%, $p < 0.01$) groups (Fig. 2C).

The results of the repeated measures ANOVA ($F(24,358 = 22.1$, $p < 0.001$) showed that chronic stress and hyperglycaemia similarly induced a deterioration of the coat state as compared to control animals, although the association of hyperglycaemia and UCMS significantly worsen the coat state (Fig. 2D).

3.2. Chronic stress, hyperglycaemia, and their association influence mice behaviour

Nest-building activity has been assessed at two time points (5 and 23 hr after the beginning of the dark phase). The nest quality of HBG and UCMS+HBG groups was clearly worse as compared to UCMS and CTRL groups (Fig. 3A).

The *open field test* showed that HBG and UCMS+HBG mice spent significantly less time in central area (Fig. 3B) preferring the corner of the arena compared to CTRL and UCMS groups. The frequency of the transition was increased in UCMS animals as compared to control, whereas a significant reduction was registered in HBG and UCMS+HBG groups compared to control and UCMS mice. In HBG animals a significant reduction of total distance covered was also recorded in comparison with all the other groups (Fig. 3B).

Tail suspension test showed that UCMS, HBG and UCMS+HBG groups developed behavioural despair that is characterized by immobility as well as the power mice' motions (energy) decreased in all groups compared to the control, while the simultaneous presence of stress and hyperglycaemia led to a significantly higher reduction of the energy (Fig. 3C).

3.3. Hyperglycaemia and its association with chronic stress could cause alterations in hippocampus energy metabolism

^{1}H-MRS spectra of the hippocampus (Fig. 4A) for CTRL, UCMS, HBG and UCMS+HBG mice highlighted the presence of the metabolites between 0.7 and 4 PPM (Fig. 4B).

Hippocampus spectra showed that UCMS did not affect metabolites concentration. (Fig. 4C).

In the HBG group, the concentrations of tNAA ($p < 0.05$), tCr ($p < 0.001$), Tau ($p < 0.001$), Gln ($p < 0.001$), Glx ($p < 0.01$) were significantly increased at the end of the experimental procedures (Fig. 4C).

Likewise, in the hippocampus of UCMS+HBG mice, the concentrations of tNAA ($p < 0.05$), tCr ($p < 0.01$), Tau ($p < 0.001$), Gln ($p < 0.001$), Glx ($p < 0.01$) were significantly increased (Fig. 4C).

Furthermore, the concentrations of tCr ($p < 0.001$), Tau ($p < 0.001$), Gln ($p < 0.001$) and Glx ($p < 0.01$) were significantly higher in HBG group than in the UCMS group, as well as the concentrations of tCr ($p < 0.001$), Tau ($p < 0.001$), Gln ($p < 0.001$) and Glx ($p < 0.01$) were significantly higher in UCMS+HBG group than in the UCMS group (Fig. 4C).

Finally, a significantly increase of the NMDAR2A expression has been observed only in the UCMS and HBG mice, compared to the control group, whereas no changes in glutamine synthase expression were detected (Fig. 4D).

3.4. Serum glucose, kynurenine, tryptophan, and kynurenine/tryptophan ratio

A significant increase of serum glucose levels was measured in HBG and UCMS+HBG animals compared to UCMS and CTRL groups, respectively (Fig. 5A).

Moreover, the kynurenine/tryptophan ratio resulted significantly increased in all experimental groups as compared to control, although in different extent. In UCMS+HBG group, the ratio was also significantly higher than that calculated in UCMS animals (Fig. 5B).

For the individual serum levels for kynurenine and tryptophan see supplementary results (Supplementary Figure 1).

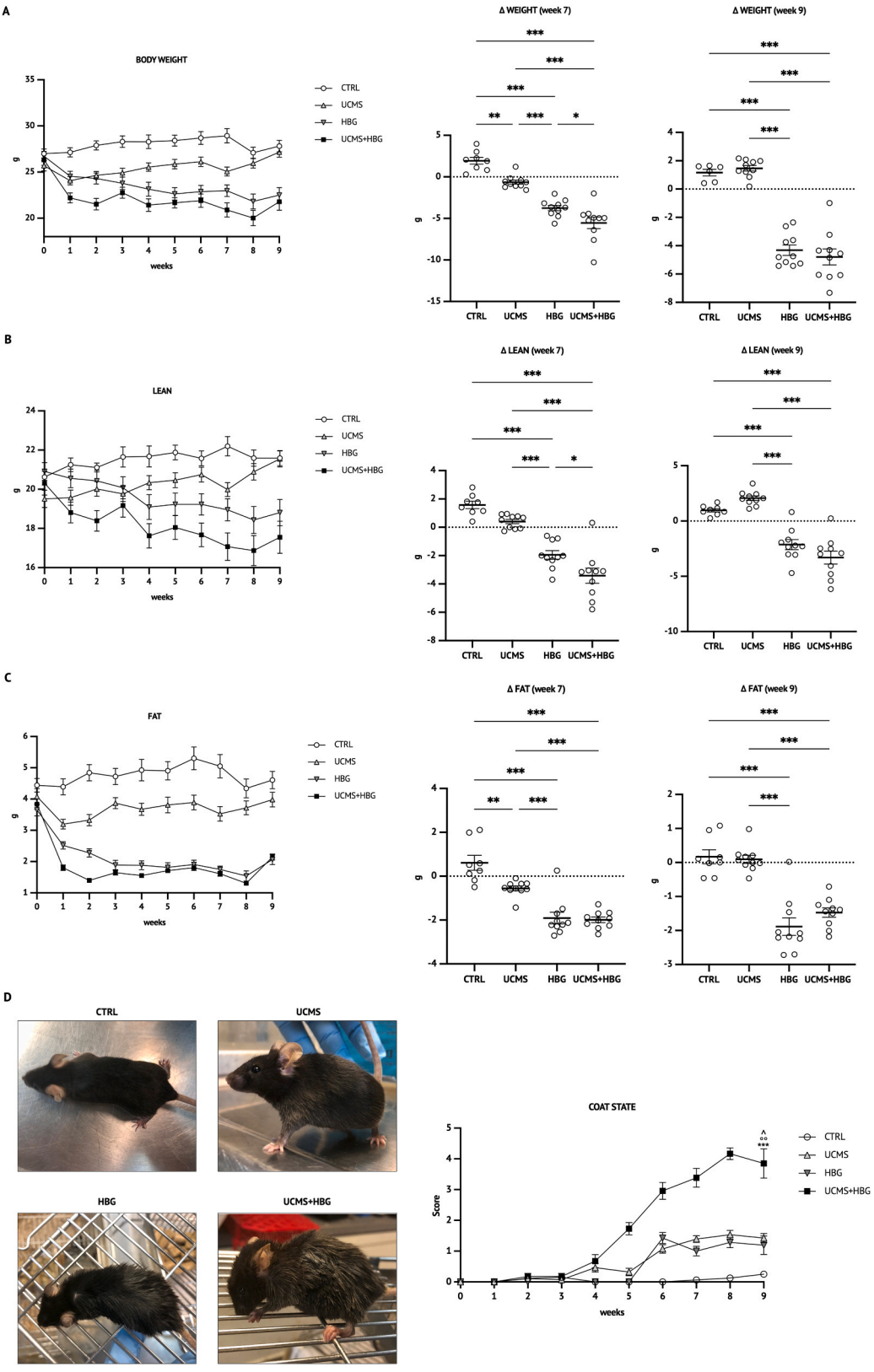

Fig. 2. Effect of unpredictable chronic mild stress (UCMS), high blood glucose (HBG) or unpredictable chronic mild stress + high blood glucose (UCMS+HBG) on (A) body weight, (B-C) body composition and (D) coat state of the mice. The loss of body weight, lean mass, and fat mass are presented as the absolute difference between baseline (week 0) and before starting behavioural tests (week 7) and at the end of the experiment (week 9). $n = 6$–10 animals/group. The results are expressed as mean ± S.E.M. Statistical analysis by one way ANOVA with Tukey's test; * : $p < 0.05$, * *: $p < 0.01$, * ** : $p < 0.001$ (A, B, C). Repeated measures ANOVA with Tukey's post hoc test; * ** : $p < 0.001$ vs CTRL; °°: $p < 0.01$ vs UCMS; ^: $p < 0.05$ vs HBG (D).

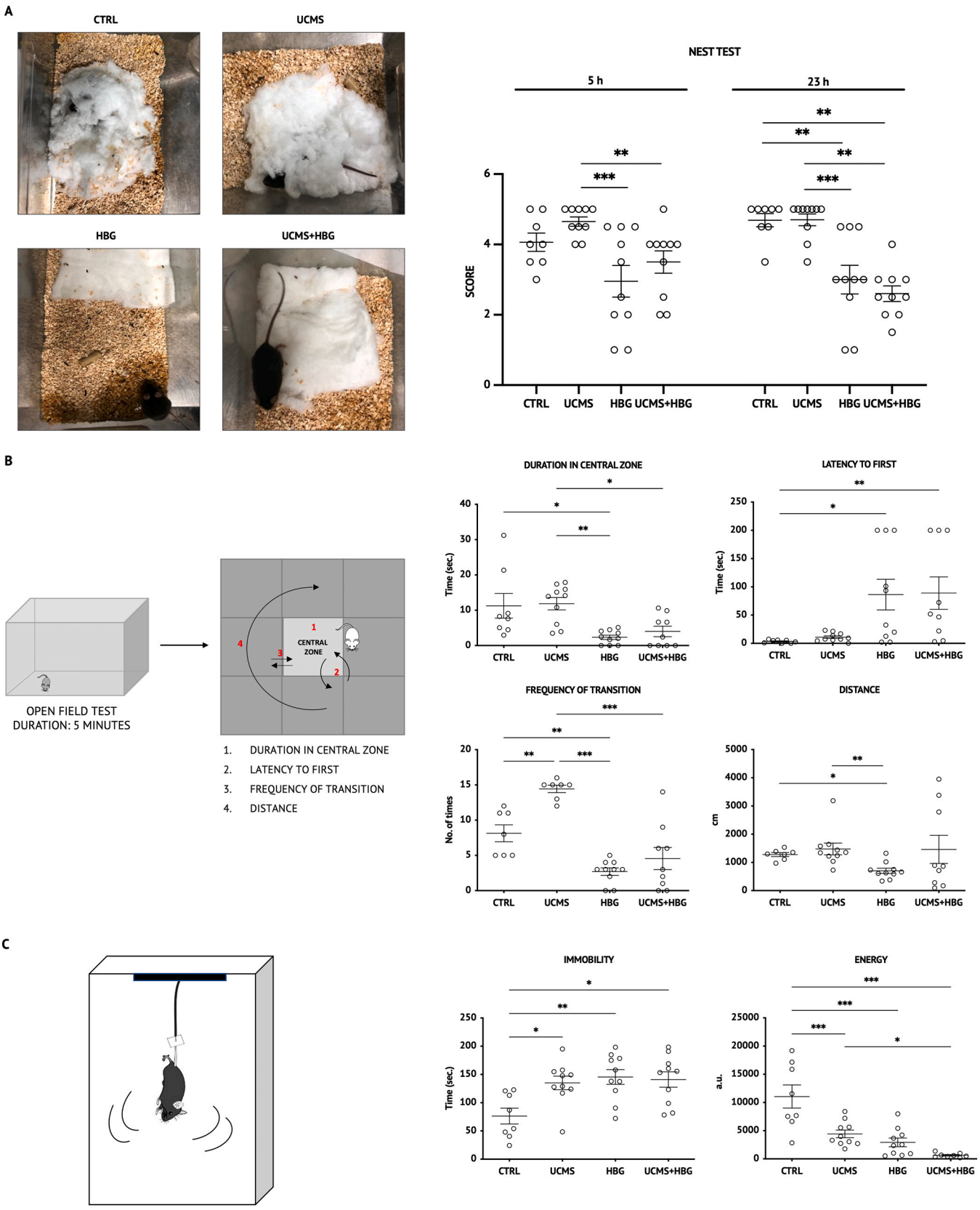

Fig. 3. Effect of unpredictable chronic mild stress (UCMS), high blood glucose (HBG) or unpredictable chronic mild stress + high blood glucose (UCMS+HBG) on mice' behaviour. (A) Nest test at 5 h and 24 h. (B) Open field test. (C) Tail suspension test. $n = 7$–10 animals/group. The results are expressed as mean ± S.E.M. Statistical analysis by one way ANOVA with Tukey's test. * : $p < 0.05$, * *: $p < 0.01$, * ** : $p < 0.001$.

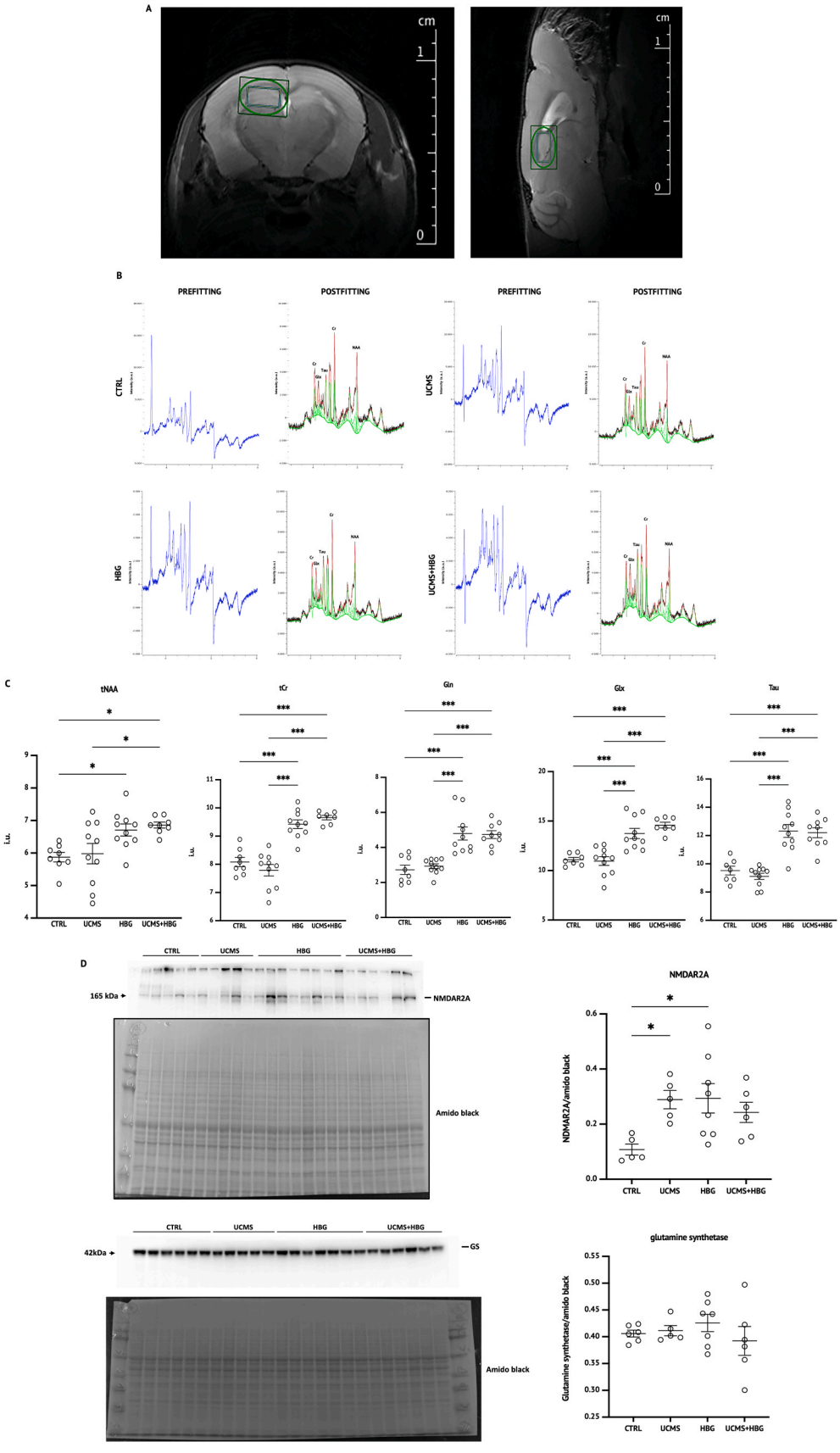

(caption on next page)

Fig. 4. Metabolic alterations of the mice' hippocampus assessed by ^{1}H-MRS and western blot analysis. (A) Representative axial and sagittal T2_turboRARE weighted images with fat suppression of mouse brain and corresponding voxel location centred in the hippocampal region (2 × 1 × 2 mm). (B) Representative in vivo pre-fitting and post-fitting ^{1}H-MRS spectra for CTRL, UCMS, HBG, UCMS+HBG mice' hippocampus performed by Tarquin. In post-fitting spectra the black trace represents the processed signal, the red trace is the model signal, while the green trace is the baseline plus the individual metabolite spectral lines. (C) Concentration values of the metabolites. tNAA, total N-acetylaspartate; tCr, total creatine; Gln, Glutamine; Glx, glutamate + glutamine; Tau, Taurine. $n = 7$–10 animals/group. The results are expressed as mean ± S.E.M. Statistical analysis by one way ANOVA with Tukey's test. * : $p < 0.05$, * ** : $p < 0.001$. (D) NMDAR2A (*N*-methyl-$_{D}$-aspartate receptor) and glutamine synthetase protein expression in the hippocampus. CTRL ($n = 5$–6); UCMS ($n = 5$); HBG ($n = 7$–8); UCMS+HBG ($n = 6$). The results are expressed as mean ± S.E.M. Statistical analysis by one way ANOVA with Tukey's test. * : $p < 0.05$.

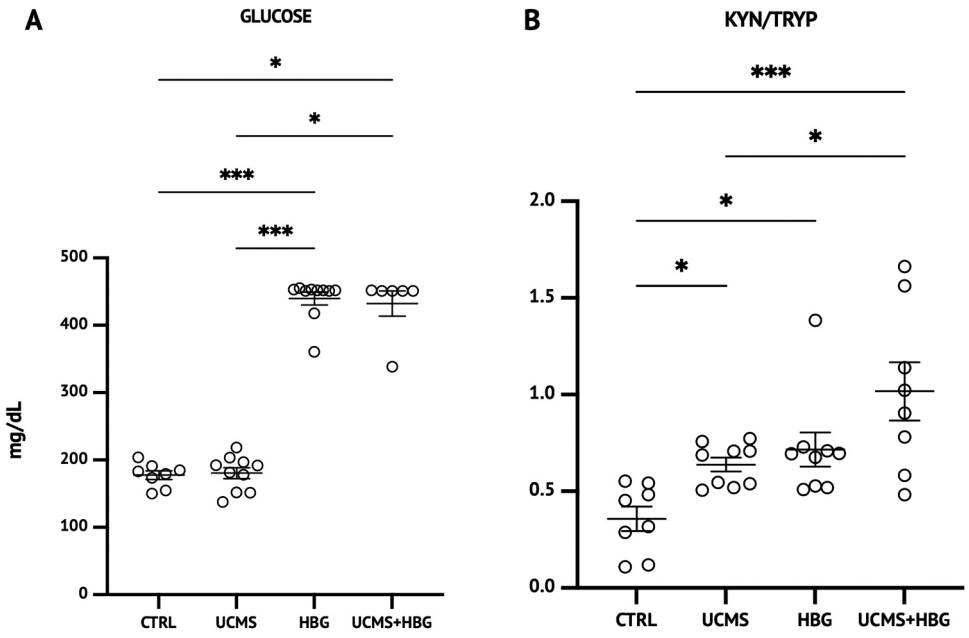

Fig. 5. Serum level quantification of (A) Glucose and (B) Kynurenine/Tryptophan ratio. The results are expressed as mean ± S.E.M. $n = 6$–10 animals/group. The results are expressed as mean ± S.E.M. Statistical analysis by Kruskal–Wallis analysis of variance followed with Dunn's test (A) and one way ANOVA with Tukey's test (B). * : $p < 0.05$, * ** : $p < 0.001$.

3.5. Hyperglycaemia and its association with chronic stress reduce total cerebral brain volume

Volumetric analysis (Fig. 6A) showed a statistically significant decrease in total cerebral brain volumes (TCBVs) for HBG mice (0.429 ± 0.004 cm^3, $p < 0.001$ vs CTRL, −6.74%) and UCMS+HBG mice (0.415 ± 0.003 cm^3, $p < 0.001$ vs CTRL, −9.78%, (Fig. 6B). Furthermore, TCBVs for both HBG and UCMS+HBG mice were significantly lower than UCMS (0.447 ± 0.006 cm^3) TCBVs ($p < 0.05$, −4.03% and $p < 0.001$, −7.16% vs UCMS respectively; Fig. 6B).

A multiple regression was performed to assess whether kynurenine or glucose serum levels could significantly affect mice TCBVs (Supplementary Figure 2). Moreover, Pearson's correlation analysis showed that the smaller TCBVs were associated with high glucose serum levels ($r = -0.60$, $p < 0.05$; Fig. 6D), whereas kynurenine serum levels were not associated with TCBVs ($r = -0.23$, $p = 0.35$, Fig. 6C).

3.6. Quinolinic acid expression and co-localization with IBA1 in hippocampus

Immunofluorescence analysis showed that UCMS or HBG led to an increase of quinolinic acid % positive pixels compared to CTRL in the hippocampus (Fig. 7A-B). The simultaneous presence of both pathological conditions led to a significant increase in all the hippocampal areas (Fig. 7A-B).

In addition, the colocalization of quinolinic acid with IBA1 was significantly higher in all the hippocampal areas of the UCMS+HBG mice compared to CTRL, UCMS and HBG mice, except for the Cornu Ammonis 1 and the dentate gyrus (Fig. 7C). The microglial activation and morphology revealed by IBA1 and DAPI staining are shown in Supplementary Figure 3.

3.7. Kynurenine expression and, kynurenine-TMEM119 colocalization in hippocampal areas

Immunofluorescence analysis showed that, in all the subareas of the hippocampus of UCMS mice, kynurenine % positive pixels were significantly higher than in the CTRL group (Fig. 8A-B). As shown in the Fig. 8C, the enhancement of kynurenine-derived signal was associated with a higher colocalization with TMEM119% positive cells, although this effect was not detected in the dentate gyrus. In addition, kynurenine % positive pixels in UCMS mice were significantly higher in the CA1, CA2 and CA3 regions than those revealed in the same hippocampal areas of HBG animals. In CA2 and CA3 regions, the colocalization with TMEM119% positive cells was significantly reduced (Fig. 8C).

In the CA1, CA3 and DG regions of HBG hippocampus, kynurenine % positive pixels were significantly higher than in the CTRL group (Fig. 8B).

Moreover, in the CA3 and DG of UCMS+HBG animals the kynurenine-associated signal was enhanced compared to the control. On the other hand, a decreased signal related to kynurenine was observed in CA1 and in CA3 areas of UCMS+HBG animals in comparison with the same hippocampal region of UCMS animals. Finally, in CA2, the signal referred to kynurenine was associated with a reduced colocalization with TMEM119 staining (Fig. 8C). The microglial activation and morphology revealed by TMEM119 and DAPI staining are shown in Supplementary Figure 4.

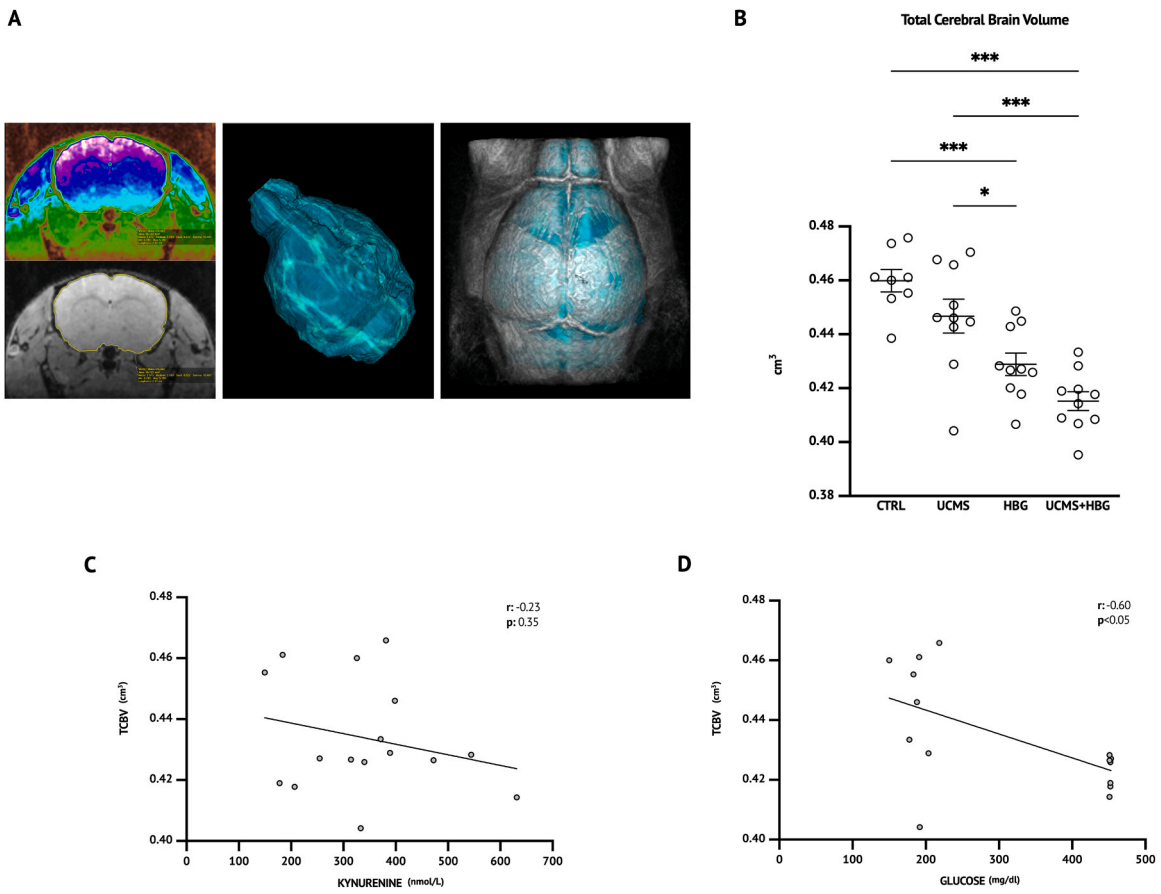

Fig. 6. Volumetric magnetic resonance imaging. (A) Representative images of volumetric analysis performed by OsiriX. (B) Total cerebral brain volume (TCBV) for the control (CTRL), unpredictable chronic mild stress (UCMS), high blood glucose (HBG), and unpredictable chronic mild stress+high blood glucose (UCMS+HBG) mice. $n = 8$–10 animals/group. The results are expressed as mean ± S.E.M. Statistical analysis by one way ANOVA with Tukey's test. * : $p < 0.05$, * ** : $p < 0.001$. (C, D) Relationship between TCBV (cm^3) and Kynurenine or Glucose serum levels performed by Pearson's correlation coefficient; lines are generated using regression analysis.

3.8. Chronic stress, hyperglycaemia and both conditions together decreased expression of astrocytic GFAP-immunoreactivity within the hippocampus

The data regarding the percentage of positive pixels, number of process endpoints and summed process length were used as measures of astrocyte activation and morphology (Fig. 9A-B).

UCMS led to a significant decrease of GFAP % positive pixels in CA1, CA2 and DG areas, as well as summed process length in the same areas (Fig. 9B). Moreover, the CA2 of UCMS animals showed a significantly decrease in the number of process endpoints (Fig. 9B).

Hyperglycaemia led to a significantly decrease of GFAP % positive pixels in the CA1, CA2 and DG areas compared to CTRL and CA1 compared to UCMS, respectively. In addition, the summed process length was significantly reduced in CA1, CA2 and dentate gyrus, as well as the number of process endpoints in CA2 (Fig. 9B).

Immunofluorescence analysis highlighted a significant reduction of GFAP % positive pixels in the hippocampus of the mice exposed to both pathological conditions. Likewise, the summed process length was significantly decreased in CA1, CA2 and dentate gyrus, as well as the number of process endpoints in CA2 region (Fig. 9B). All the pathological conditions did not affect the astrocyte activation and morphology in Cornu Ammonis 3 (Fig. 9B).

3.9. Chronic stress, hyperglycaemia and co-occurrence of both conditions alter mitochondrial protein expression

A western blot analysis was performed to evaluate changes in the expression of proteins involved in mitochondrial function. A significant reduction of Drp1 phosphorylation at Ser-637 has been observed in the mice exposed to UCMS, hyperglycaemia or to both conditions (Fig. 10A). Likewise, OPA1 levels were significantly decreased in the mice that underwent chronic stress, hyperglycaemia or both conditions (Fig. 10B). Notably, nNOS expression was significantly upregulated in UCMS+HBG mice compared to control group as well as in in HBG and UCMS+HBG groups compared to UCMS mice (Fig. 10C). Furthermore, MnSOD expression was significantly downregulated in both HBG or UCMS+HBG animals compared to CTRL and UCMS mice (Fig. 10D). GLUT-4 levels were significantly reduced by hyperglycaemia associated with UCMS compared to CTRL, UCMS and HBG, respectively (Fig. 10E). Moreover, a significant reduction in the levels of VDAC1 and NADPH OXIDASE 4 has been detected in the HBG and UCMS+HBG groups compared to the control group (Fig. 10F-G). Finally, NADPH OXIDASE 4 was significantly lower in the HBG and UCMS+HBG animals than UCMS animals (Fig. 10G).

3.10. Chronic stress, hyperglycaemia and the simultaneous presence of both conditions alter neuronal structure, density, and induce neuronal damage in hippocampus

To assess the effect of UCMS, HBG and the association of both

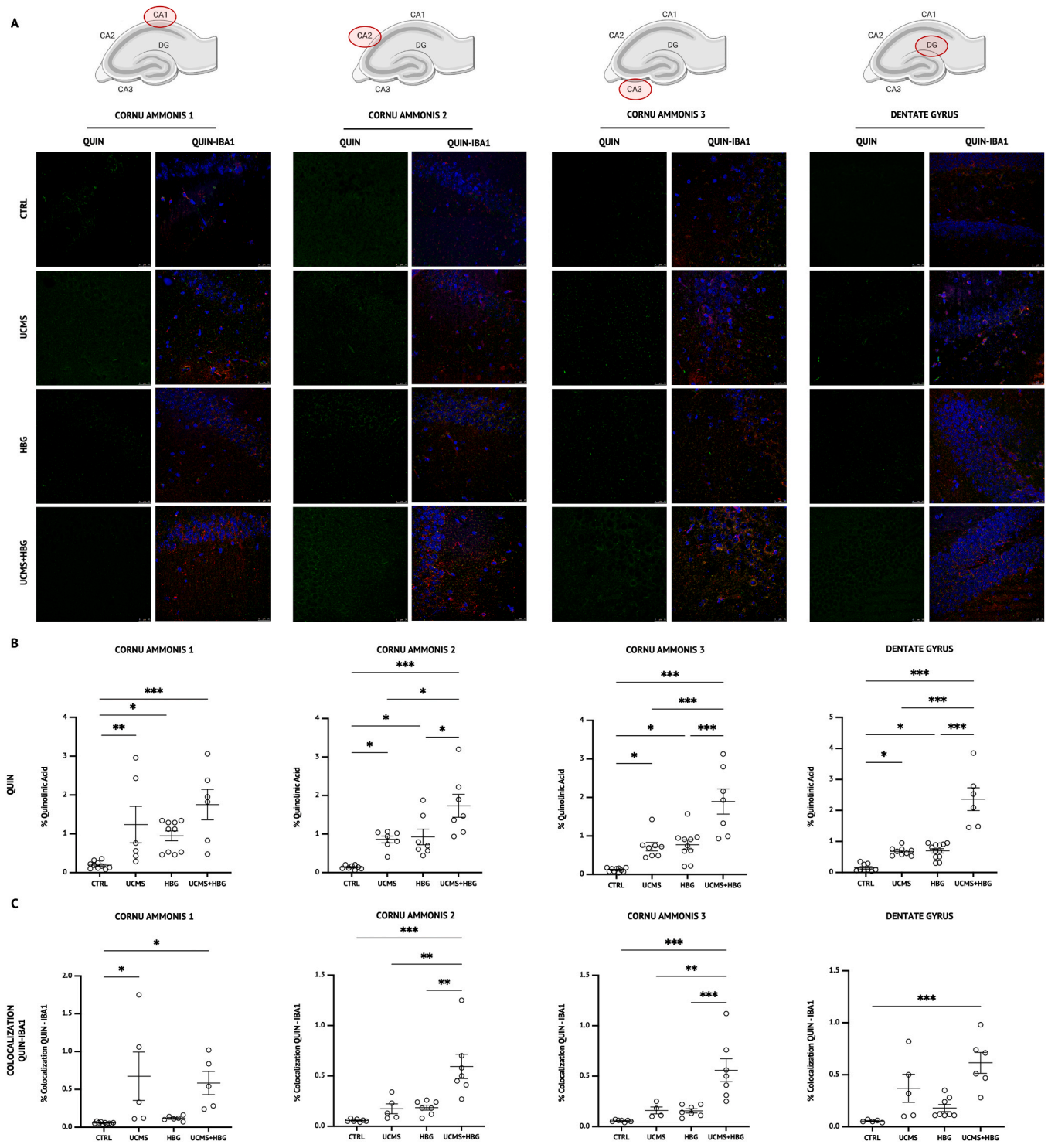

Fig. 7. Immunofluorescence staining for Quinolinic Acid (QUIN) and colocalization between QUIN and IBA1 in microglia. (A) Representative confocal images and quantification for QUIN % positive and Colocalization of QUIN-IBA1 in Cornu Ammonis 1, Cornu Ammonis 2, Cornu Ammonis 3, and Dentate Gyrus. The microglial activation and morphology revealed by IBA1 and DAPI staining are shown in Supplementary Figure 3. (B, C) Percentage of Quinolinic Acid and Colocalization with IBA1. The results are expressed as mean ± S.E.M. $n = 4$–10 animals/group. Statistical analysis by one way ANOVA with Tukey's test. * : $p < 0.05$, * *: $p < 0.01$, * **: $p < 0.001$.

conditions on the neuronal health we measured the neuronal densities in all hippocampal regions (Fig. 11A-B). Immunofluorescence analysis showed a significant decrease of TUBB3% positive pixels, number of process endpoints, summed process length, and soma area, in all hippocampal regions (CA1, CA2, CA3 and DG) of UCMS, HBG and UCMS+HBG compared to the control animals (Fig. 11B).

The DNA fragmentation is one of the peculiar markers for apoptosis. To assess the hypothetical apoptotic damage due to UCMS, HBG or to the association of both conditions, a TUNEL assay has been performed (Fig. 12A). Results showed that UCMS, HBG and UCMS+HBG led to abundant TUNEL positive cells in CA1, CA2 region and dentate gyrus, compared to CTRL group whereas a significantly increase of TUNEL

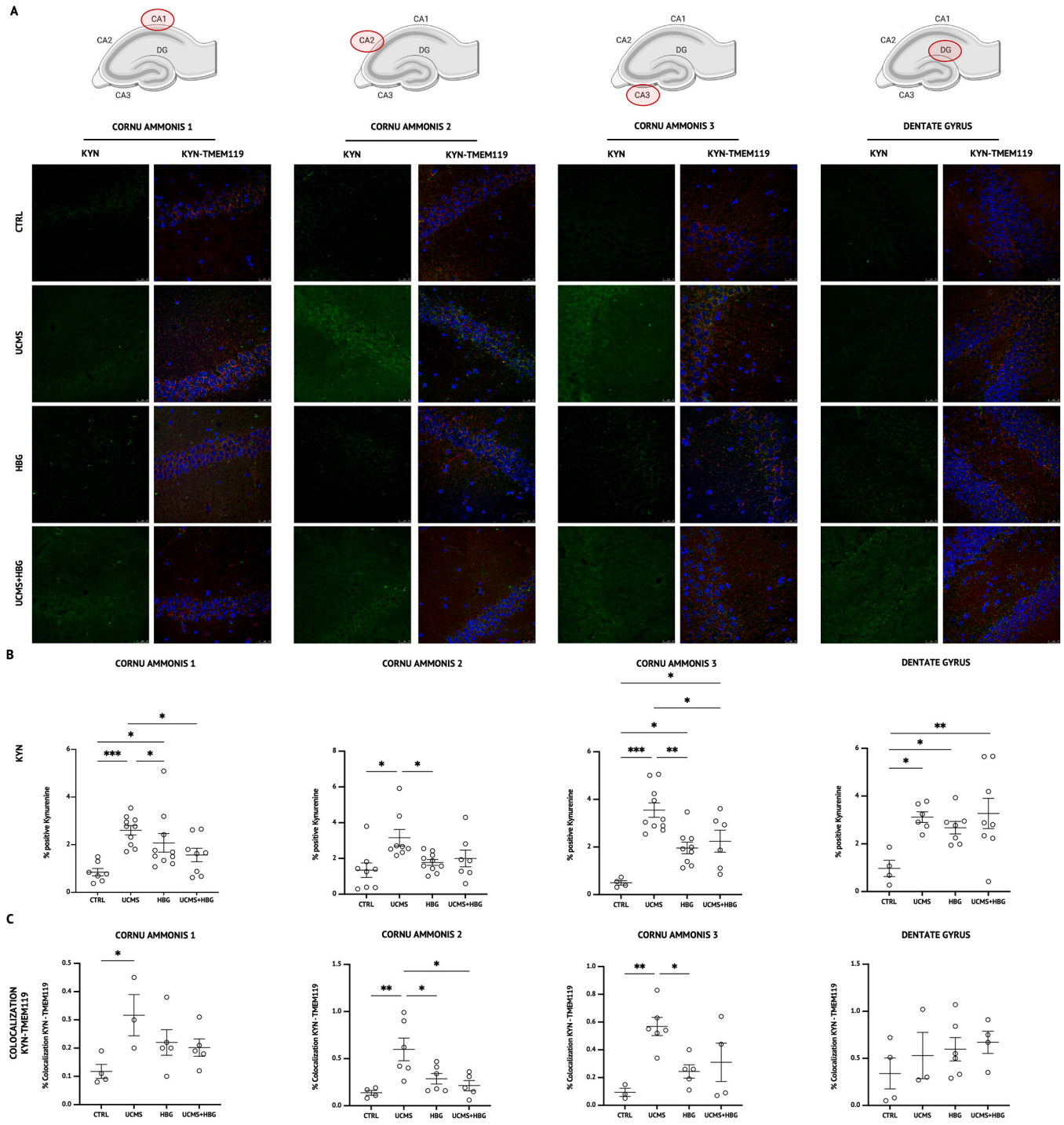

Fig. 8. Immunofluorescence staining for Kynurenine (KYN) and colocalization between KYN and TMEM119 in microglia. (A) Representative confocal images and quantification for KYN % positive and Colocalization of KYN-TMEM119 in Cornu Ammonis 1, Cornu Ammonis 2, Cornu Ammonis 3, and Dentate Gyrus. The microglial activation and morphology revealed by TMEM119 and DAPI staining are shown in Supplementary Figure 4. (B, C) Percentage of Kynurenine Acid and Colocalization with TMEM119. The results are expressed as mean ± S.E.M. $n = 3$–10 animals/group. Statistical analysis by one way ANOVA with Tukey's test. * : $p < 0.05$, * *: $p < 0.01$, * ** : $p < 0.001$.

positive fragments have been observed in CA3 region of HBG and UCMS+HBG (Fig. 12B). Furthermore, the expression of VEGF-A, an important signalling protein involved in the growth and maintenance of both vascular and neural cells, has been investigated. Results showed a down regulation of the protein in UCMS animals compared to CTRL, HBG and UCMS+HBG group (Fig. 12C). Finally, as shown in Fig. 11D the UCMS+HBG mice had reduced BDNF protein expression ($p < 0.05$) compared to the control (Fig. 12D).

4. DISCUSSION

Several epidemiological studies highlighted a bi-directional relationship between depressive symptoms and diabetes mellitus [50–55], suggesting the existence of common molecular mechanisms underlying them. However, despite this growing evidence and the emergent need to treat this comorbidity as a separate entity than two different diseases [56,57], the pathogenic mechanisms underlying it have not been clearly

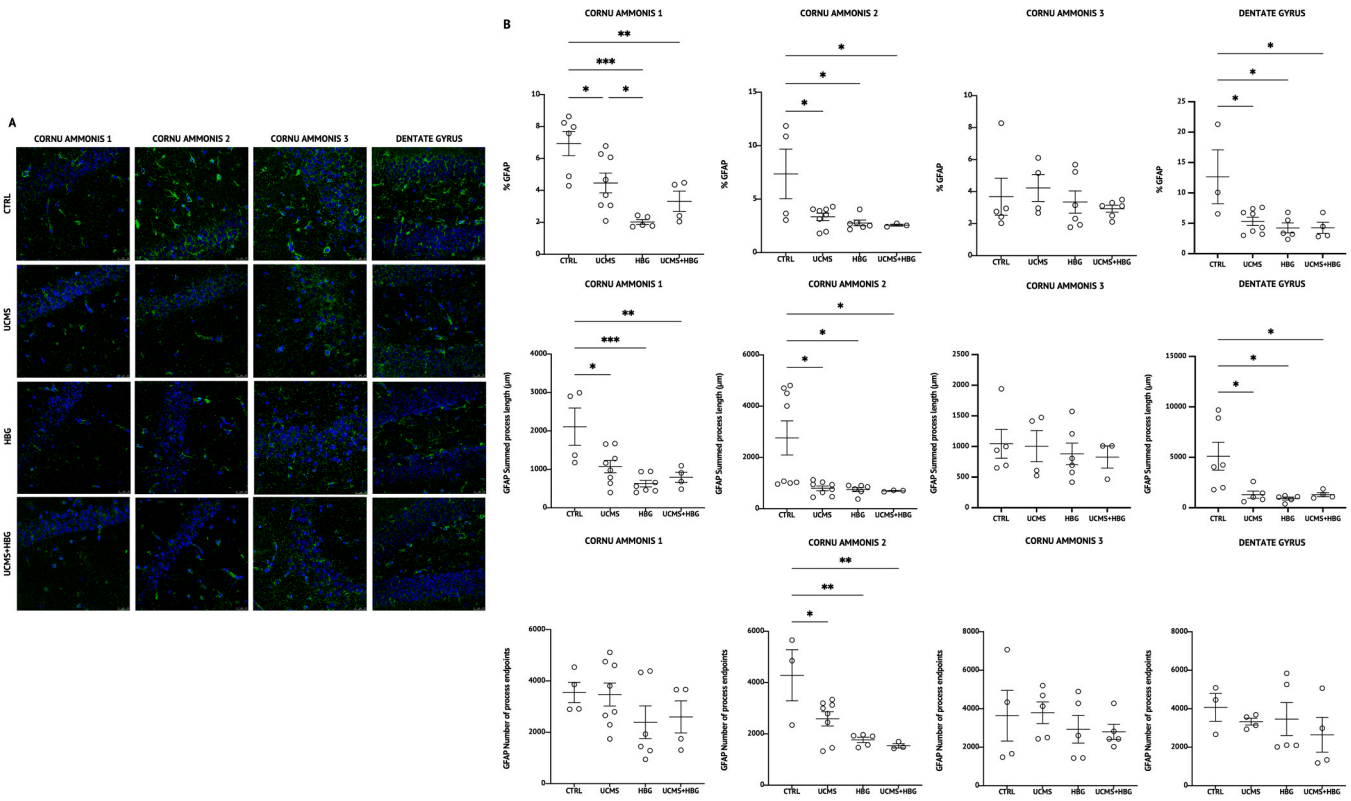

Fig. 9. Immunofluorescence staining for GFAP in astrocytes. (A) Representative confocal images of GFAP (Glial Fibrillary Acidic Protein) positive astrocytes in Cornu Ammonis 1, Cornu Ammonis 2, Cornu Ammonis 3, and Dentate Gyrus. (B) The results are expressed as mean ± S.E.M. $n = 3–8$ animals/group Statistical analysis by one way ANOVA with Tukey's test. * : $p < 0.05$, * *: $p < 0.01$, * ** : $p < 0.001$.

identified.

Our work demonstrates that KP dysregulation, leading to apoptosis in the hippocampus, can be differently triggered by hyperglycaemia and chronic stress. Specifically, the former can promote the infiltration of peripheral mediators of inflammation through blood brain barrier (BBB) and the consequent release of kynurenine; the latter mediates peripheral kynurenine overproduction that, crossing BBB, promotes resident microglia activation; both mechanisms finally determine the dysfunction of glutamate neurotransmission. In this scenario, QA, derived from kynurenine catabolism, appears a key mediator causing glutamatergic synapse dysfunction and apoptosis, thus contributing to brain atrophy. Surprisingly, we demonstrated for the first time that the coexistence of hyperglycaemia and chronic stress worsens hippocampal damage, potentiating or abating some effects, and activating alternative mechanisms that might evoke the compromission of neurogenesis.

In the recent years, it has been revealed that the impaired KP homeostasis, underlying the activation of inflammatory processes, is directly connected to the detrimental effects of chronic hyperglycaemia [58] on central nervous system, according with increasing evidence that supports the compromission of mental and physical wellbeing in diabetic patients [56,57,59–65]. Our experiments showed that the increased serum glucose levels in HBG mice were associated with a significant enhancement in kynurenine/tryptophan (KYN/TRY) ratio as compared to the control group and that HBG induced an increased kynurenine-related signal in CA1, CA3 and DG areas of the hippocampus. This is in accordance with the literature reporting that the increased influx of TRY and KYN in the brain [29,66,67], often aided by enhanced permeability of BBB and by infiltration of macrophages, can cause an excess of kynurenine in the brain parenchyma that, in turn, stimulates KP in activated microglial cells [68]. In accordance with this hypothesis, we detected an increase of positive cells for the microglial marker ionized calcium binding adaptor molecule 1 (IBA1) in CA1 and CA2 regions. Moreover, cellular morphology indicated that the proliferation of microglia was associated with a boosted differentiation of infiltered monocytes in a macrophagic phenotype [69], as shown by the enhanced trend of the process endpoint number also in CA3 and DG areas. These signs of inflammation were additionally confirmed by the amplification of taurine levels measured through ^{1}H-MRS spectroscopy analysis.

In activated immune cells, QA, derived from KYN catabolism, can accumulate to produce a reserve of NAD^{+} aimed to prevent DNA damage induced by oxidative stress [70], and to ensure mitochondrial dynamics and function modulating ROS and ATP production [70]. On the other hand, after excretion from immune cells, QA can affect mitochondrial function in neurons [71] and the inflammatory status due to hyperglycaemia, overall, can affect the entire neurovascular unit (NVU) [72–75]. To verify the possible influence of HBG induced-QA on glutamatergic synapse, energetic status, and mitochondrial function, we firstly quantified total N-acetylaspartate (tNAA), deriving from the sum of NAA and N-acetylaspartylglutamate (NAAG).

In neuronal cytosol, NAA can be employed as precursor of N-acetylaspartylglutamate (NAAG) that is transported in astrocytes and ultimately hydrolysed to produce NAA and L-glutamate [76,77]. Furthermore, tNAA favours the transfer of reducing equivalents, needed to tricarboxylic acid (TCA) cycle reactions, into neuronal mitochondria matrix exploiting the malate/aspartate shuttle cycle [78]. In HBG animals, we detected an increase in tNAA, suggesting that it served to ensure glutamate required to neurotransmission; moreover, we hypothesized that it was able to counteract the impairment of mitochondrial function and metabolism. In accordance with this theory, in HBG animals, we measured enhanced levels of glutamine (Gln) and glutamine+glutamate (Glx) as compared to control, although no changes in glutamine synthase expression were detected. However, despite at presynaptic level glutamate homeostasis appeared to be preserved, a raised expression of NR2A subunit of the glutamate NMDA receptor suggested

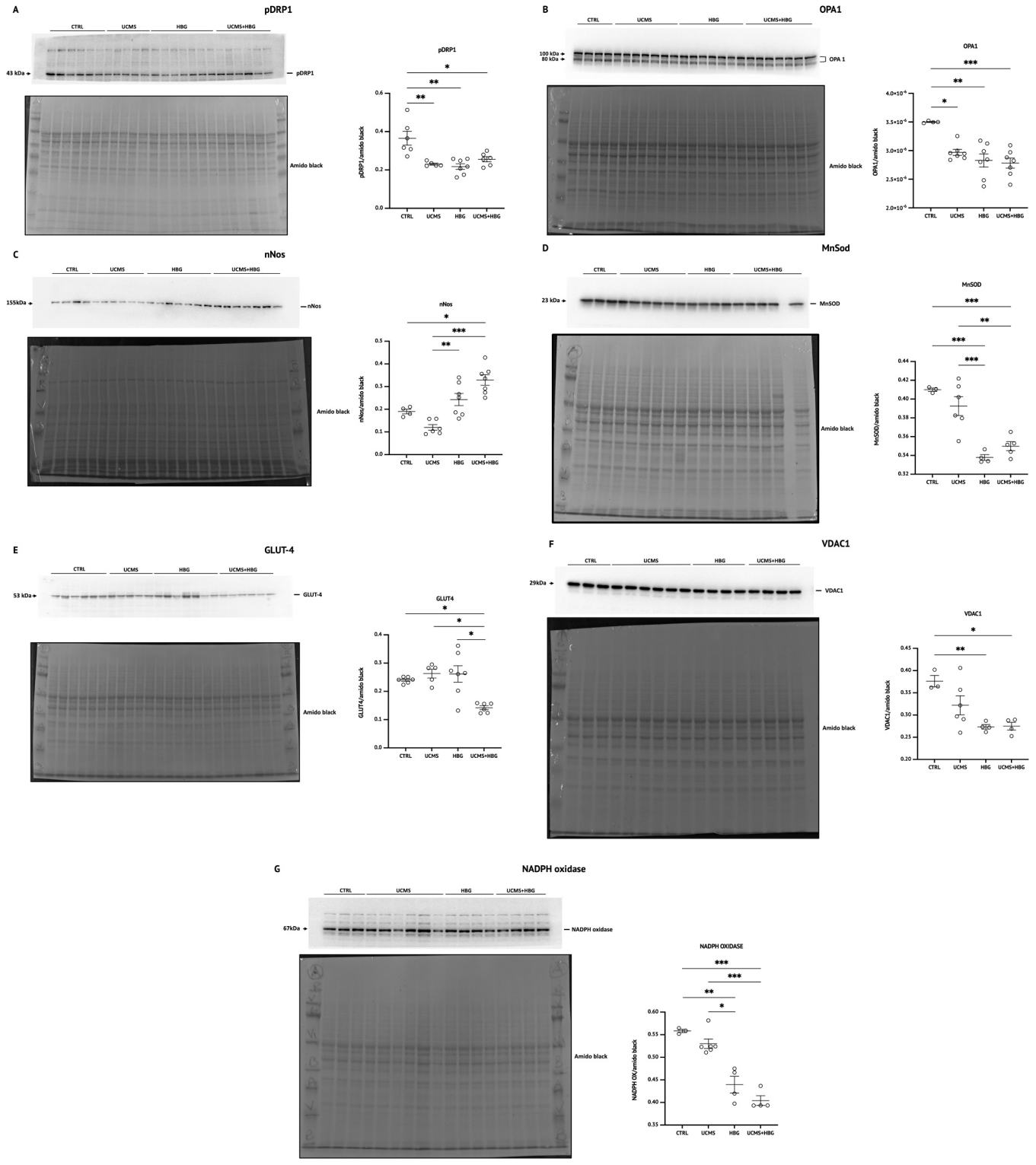

Fig. 10. Expression of proteins involved in mitochondrial function evaluated by western blot analysis. The results are expressed as mean ± S.E.M. Statistical analysis by one way ANOVA with Tukey's test. * : $p < 0.05$, * *: $p < 0.01$, * ** : $p < 0.001$. (A) pDRP1: phospho dynamin-related protein 1; CTRL ($n = 6$); UCMS ($n = 5$); HBG ($n = 7$); UCMS+HBG ($n = 6$). (B) OPA1: protein optic atrophy 1; CTRL ($n = 4$); UCMS ($n = 7$); HBG ($n = 7$); UCMS+HBG ($n = 7$). (C) nNos: ***n***itric oxide synthases**;** CTRL ($n = 4$); UCMS ($n = 6$); HBG ($n = 7$); UCMS+HBG ($n = 7$). (D) MnSOD: manganese superoxide dismutase; CTRL ($n = 3$); UCMS ($n = 6$); HBG ($n = 4$); UCMS+HBG ($n = 5$). (E) GLUT-4: Glucose transporter type 4; CTRL ($n = 6$); UCMS ($n = 5$); HBG ($n = 7$); UCMS+HBG ($n = 6$). (F) VDAC1: voltage-depende***n***t anion channel 1; CTRL ($n = 3$); UCMS ($n = 6$); HBG ($n = 4$); UCMS+HBG ($n = 4$). (G) NADPH oxidase. CTRL ($n = 3$); UCMS ($n = 6$); HBG ($n = 4$); UCMS+HBG ($n = 4$).

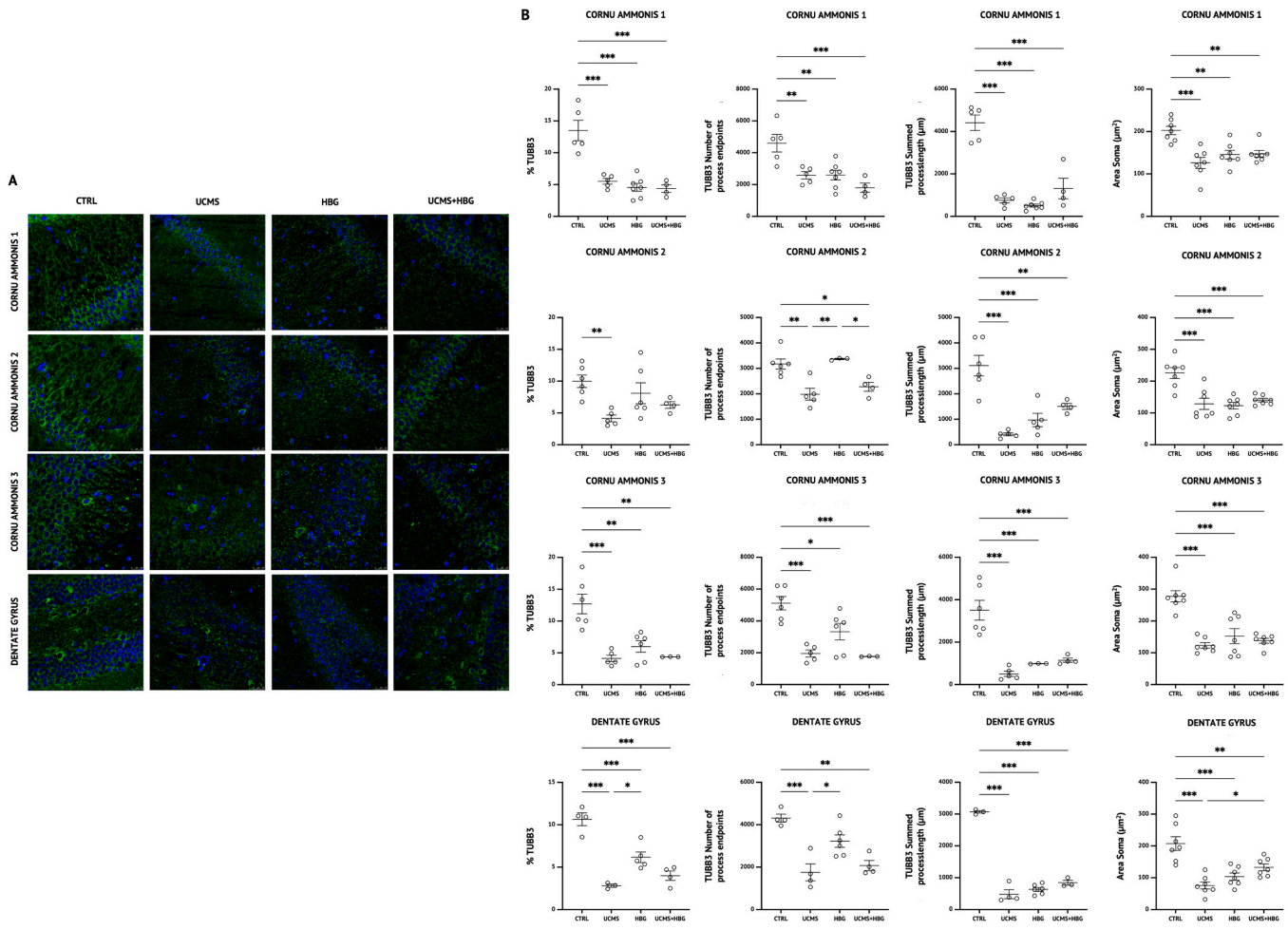

Fig. 11. Immunofluorescence staining for TUBB3 in neurons. (A) Representative confocal images of TUBB3 positive neurons in Cornu Ammonis 1, Cornu Ammonis 2, Cornu Ammonis 3, and Dentate Gyrus. (B) Quantification of TUBB3 (anti-β III Tubulin). The results are expressed as mean ± S.E.M. $n = 3–7$ animals/group. Statistical analysis by one way ANOVA with Tukey's test. * : $p < 0.05$, * *: $p < 0.01$, * ** : $p < 0.001$.

its overstimulation in postsynaptic neurons. Effectively, the significant increase of QA levels in HBG hippocampus in comparison with control appeared to mean that its excretion from immune cells, after KYN catabolism, determined the binding with NMDA receptors as competitive agonist, leading to mitochondrial dysfunction and neuronal damage [71,79–81]. The morphological analysis of neurons confirmed the occurrence of cellular damage, showing a significant down-regulation of the neuronal marker β-tubulin III in CA1, CA3 and DG areas. This reduction was associated with a decreased number of the process endpoints, summed process length and soma area in all hippocampal regions, clearly indicating the existence of cellular suffering and the loss of neuronal connections preceding cell death. In this scenario, total hippocampal energetic status was assessed quantifying total creatine levels (creatine+phospho-creatine) considered a phosphate reserve aimed to synthetize ATP [82,83]. Although our experiments showed highest levels of total creatine than in control, highlighting a raised metabolic demand, the down-expression of VDAC1 suggested a decreased exchange of metabolites (i.e., pyruvate, malate, succinate, $NADH/NAD^+$) across the outer mitochondrial membrane [84,85], implying a reduced respiratory capacity [86]. Mitochondrial dysfunction was further reflected by the significant reduction of Drp1 phosphorylation at Ser-637 and of OPA1 expression, indicating the activation of mitochondrial fission [75], other than by the decreased MnSOD levels, denoting a reduction of superoxide radical anion scavenging [40]. These detrimental effects of QA at postsynaptic level finally induced cell death as shown by the significant enhancement of TUNEL positive cells in all regions of hippocampus as compared to control.

KP dysregulation also influenced astrocytes, suggesting the involvement of the entire NVU. Particularly, the significant decrease of GFAP % positive pixels and of the summed process length limited to CA1, CA2 and DG areas of the hippocampus, was associated with a reduction of the number of process endpoints in CA2 area, probably indicating the astrocytic activation caused by infiltered monocytes, but also the reduction of inward extensive neuromodulatory projections from DG [87] that represents the most damaged area. These peculiar morphological changes in astrocytes, not involving CA3, are distinctive of the early non-proliferative astrogliosis preceding atrophy, that is characterized by an only partial loss of cellular function contributing to the reduction in synaptic coverage [88–90].

As KP dysregulation represents a relevant player in the development of neuroinflammation underlying major depressive disorder induced by chronic stress [91–93], we also examined the impact of QA in the hippocampus of UCMS mice. Although we measured a significant increase in plasma KYN/TRY ratio in comparison with control, a different modulation of kynurenine concentrations than those observed in the hippocampus of HBG animals was revealed. Indeed, enhanced levels of KYN were detected in all areas; moreover, in CA1, CA2 and CA3, this pattern of expression was accompanied by a significant enhancement of its colocalization with positive cells for TMEM119, a specific transmembrane protein expressed by resident microglia but not by blood-derived macrophages. Therefore, we hypothesize that the proliferation of local microglia was directly driven by peripheral kynurenine

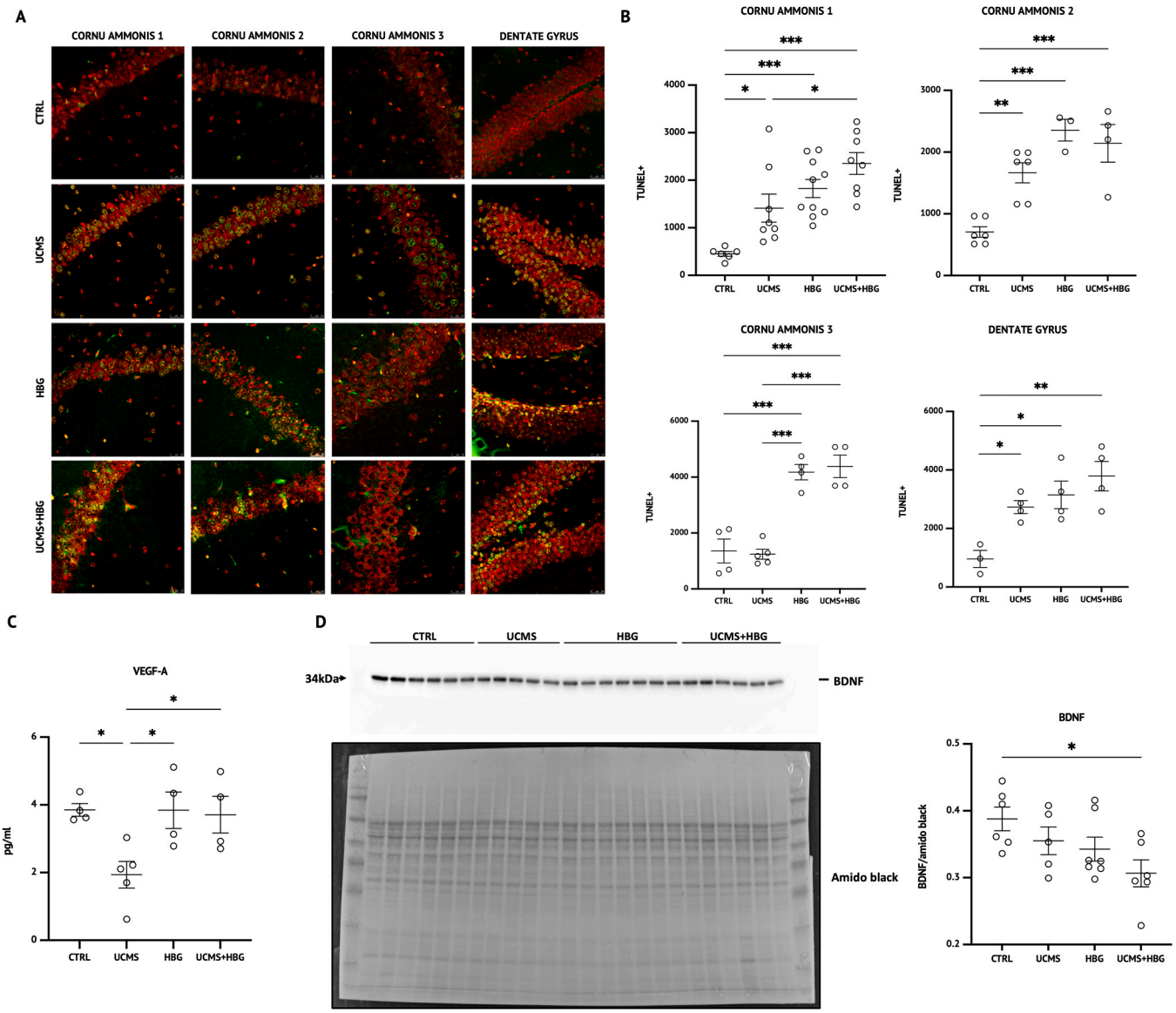

Fig. 12. Immunofluorescence staining for TUNEL+ fragments as cells apoptosis assessment. The results are expressed as mean ± S.E.M. Statistical analysis by one way ANOVA with Tukey's test. (A) Representative confocal images of TUNEL+ fragments in Cornu Ammonis 1, Cornu Ammonis 2, Cornu Ammonis 3, and Dentate Gyrus. TUNEL: TdT-mediated dUTP Nick-End Labeling. (B) Quantification of TUNEL+ fragments. $n = 3$–10 animals/group. * : $p < 0.05$, * *: $p < 0.01$, * ** : $p < 0.001$ (C) Expression of VEGF-A (vascular endothelial growth factor A). $n = 4$–5 animals/group. * : $p < 0.05$. (D) BDNF (Brain-derived neurotrophic factor) protein expression in the hippocampus. CTRL ($n = 6$); UCMS ($n = 5$); HBG ($n = 7$); UCMS+HBG ($n = 6$). * : $p < 0.05$.

production. The peculiar localization of KYN-related signal was also associated with enhanced levels of QA as well as with the highest increase in NR2A expression than in control. Furthermore, the significant reduction of Drp1 phosphorylation at Ser-637 and OPA1 levels in the mice subjected to chronic stress indicated a compromised mitochondrial function responsible for excitotoxicity [94].

Conforming to this hypothesis, the morphological analysis of neurons showed a compromission of their structure as well as a down-regulation of the neuronal marker β-tubulin III in all hippocampal areas that, in CA1, CA2 and DG zones, was associated to an augmented apoptotic cell death. Differently from hyperglycaemic animals, the impaired neuronal status was characterized by a decreased VEGF expression, suggesting a down-regulation of neurogenesis caused by the chronic stress [95], that needs to be verified through further studies. Overall, these results reflected the presence of NVU changes, also highlighted by the degeneration in the morphological complexity and length of astrocytes in the same areas of HBG animals [96,97], although in CA2 astrocyte activation was due to the resident microglia.

The lack of the NVU integrity resulting from the concomitance of hyperglycaemia and UCMS, revealed unexpected elements. Indeed, it concealed the activation of original mechanisms leading to neuronal damage and hippocampal dysfunction, that were alternatively associated with the potentiation or by the deletion of some typical features of HBG or UCMS.

First, the increased KYN/TRY ratio was amplified in the UCMS+HBG mice than in other groups and was associated with an enhanced KYN catabolism as shown by the highest levels of measured QA. The development of hippocampal inflammation, also denoted by the increased taurine levels, was characterized by the most marked changes in microglia morphology and IBA1 expression in the entire hippocampus. Although this result suggested a widespread macrophage infiltration driven by chronic hyperglycaemia, CA3 zone was particularly affected by the activation of resident microglia (TMEM119 positive cells), typically observed in UCMS animals.

This inflammatory framework targeted astrocytes and neurons. Indeed, the decreased expression of astrocytic GFAP-immunoreactivity

and the reduction of the sum of process length and of the number of endpoints denoted the onset of astrocyte atrophy, whereas the significant down-regulation of the neuronal marker β-tubulin III in all hippocampal areas showed a prominent neuronal injury in UCMS+HBG in comparison with the other groups. In this scenario, we also observed specific signs underlying the impairment of the energy metabolism difference between astrocytes and neurons [98], characterized by their dependence on mitochondrial oxidative phosphorylation for survival [99]. Specifically, we have detected an enhanced expression of neuronal nitric oxide (NO) synthase (nNOS) in HBG and UCMS+HBG groups, suggesting that the increased production of NO, due to hyperglycaemia, could contribute to the maintenance of astrocyte mitochondrial membrane potential, eluding apoptosis. On the other hand, the raised levels of neuronal NO and superoxide anions, following the down-expression of MnSOD, could induce the dysfunction of mitochondrial respiratory chain, the increased formation of peroxynitrite [100] and the promotion of neuronal injury leading to cell death. This is supported by literature evidence showing that astrocytes can higher withstand the inhibition of mitochondrial complex IV caused by nitric oxide (NO) [99,101–103], upregulating AMPK-dependent glycolysis [99] and partially counterbalancing the loss of ATP needed to maintain the mitochondrial membrane potential and to evade apoptosis [104]. By contrast, the suppression of oxidative phosphorylation in neurons is not able to activate glycolysis similarly [99], thus provoking ATP depletion, mitochondrial membrane potential collapse and cell death [101,104]. Actually, in our experiments, the hypothesized compromission of glycolysis was associated with the down expression of GLUT-4, a transporter specifically expressed in stressful neurons requiring an increased energy demand [98]; whereas, we postulate that the worsened metabolism in astrocytes, manifested as an impairment of glucose storage featuring the onset of atrophic process [89,105], resulting in the dysregulation of energy supply to neurons [98,106–108]. This is in line with the amount of tNAA, tCr, Gln and Glx denoting the utilization of glutamate as energetic fuel, at the expense of glutamatergic synapse, as observed in HBG group; on the other hand, in UCMS+HBG, the oxidative damage triggered by the highest increase in QA levels appeared both partially dependent from NMDA activation [81], as shown by the trend in NR2A overexpression, and from the down-regulation of GLUT-4 [109]. Thus, the simultaneous exposition to HBG and UCMS could have exacerbated the changes in glycolytic metabolism observed under the single pathological conditions and led to a reduction in mitochondrial respiration. Although it could be counterbalanced by the need of higher levels of cytosolic NAD+ derived from QA as substrate, our results highlighted that QA overproduction was finalized to mitochondrial dysfunction rather than to a protective role. Indeed, we observed lowered levels of NOX4 and MnSOD, probably involved in the down-regulation of OPA1 and Drp-1 phosphorylation at Ser 637, respectively [110,111]. The consequent neuronal suffering, highlighted by the alteration of cellular morphology, fell within a broader context of hippocampal damage characterized by the highest degree of apoptotic cell death, especially in CA3 area, as compared to the other groups, and by the down-expression of the brain derived nerve factor (BDNF). In the early stages of stress-induced major depression [112,113], BDNF down-regulation is involved in the alteration of neuron survival and proliferation of new-born neurons [114]. Hence, the reduction of its expression in UCMS+HBG group, versus the unchanged levels observed in UCMS animals at the end of the experiment, suggest that hyperglycaemia-induced inflammation might contribute to compromise neuronal genesis/trophism via BDNF downregulation for longer times. Finally, in this alternated prevalence of detrimental effects induced by hyperglycaemia and UCMS, in UCMS+HBG animals, brain atrophy was driven by HBG-induced inflammation, as shown by the heavily reduction of total brain volume. Altogether, these mechanisms translated into depressive-like symptoms [115–118] highlighted by the worsening of the coat state, the alteration of body weight and body composition as well as by the performed behavioural tests. Specifically, the fear/anxiety behaviour [119], that in UCMS animals manifested as hyperactivity, worsened the signs of despair-like behaviours [120] observed in HBG group. Indeed, in UCMS+HBG animals, the energy associated with the decreased locomotor activity was markedly reduced and the time of animal immobility was increased. Moreover, the apathy-like behaviour [121] typical of HBG mice was worsened overtime by UCMS stimulus, despite the initial tendency of stressed animals was to build the best structured nest to escape to safety [122].

5. CONCLUSION

Despite the link between psychological stress and diabetes has long intrigued the scientific community [8,12], because both pathologies can affect mental and physical wellbeing [56,57,59–65,123] to date, neurodegenerative mechanisms underlying their association, beyond oxidative stress and cytokine overproduction, have not been elucidated, although emerging evidence supports a beneficial effects of some antidepressants in the management of depressive symptoms and the high blood glucose control [124]. Our results show that in the development of the peculiar disease due to this comorbidity, hyperglycaemia/chronic stress interaction resembles the interchanging of the prevalent role between two partners dancing the “West Coast Swing”. Indeed, we discovered that in the various aspects characterizing NVU impairment, the leading contribution of hyperglycaemia or chronic stress can sum or can originate different effects than those observed under the single diseases. Thus, the real novelty of our work is represented by the characterization of the rules and the steps of this dangerous dance for human health, that can open new perspectives for a personalized management of diabetic/depressed patients, but also for the comprehension of the molecular mechanisms underlying other neurodegenerative disease characterized by the compromission of hippocampal function.

Funding

- PON-MIUR 03PE000_78_1 and PONMIUR 03PE000_78_2/Ministry of Education, Universities and Research.
- PRIR Calabria Asse 1/Azione 1.5.1/FESR (Progetto AgrInfra Calabria)./PRIR Calabria.
- Open access funding provided by Università degli Studi Magna Graecia di Catanzaro within the CRUI-CARE Agreement.

CRediT authorship contribution statement

Carresi Cristina: Visualization, Supervision, Software, Investigation, Formal analysis, Data curation. **Nucera Saverio:** Investigation. **Ruga Stefano:** Investigation. **Scarano Federica:** Investigation. **Bosco Francesca:** Investigation. **Guarnieri Lorenza:** Investigation. **Macrì Roberta:** Investigation. **Mollace Rocco:** Investigation. **Gliozzi Micaela:** Writing – review & editing, Writing – original draft, Supervision, Project administration, Methodology, Investigation, Formal analysis, Data curation, Conceptualization. **Belzung Catherine:** Writing – review & editing, Writing – original draft, Visualization, Supervision, Project administration, Investigation, Data curation, Conceptualization. **Coppoletta Anna Rita:** Writing – review & editing, Writing – original draft, Visualization, Software, Investigation, Formal analysis, Data curation. **Mollace Vincenzo:** Visualization, Supervision, Project administration, Investigation, Data curation, Conceptualization. **Cardamone Antonio:** Writing – review & editing, Writing – original draft, Visualization, Software, Investigation, Formal analysis, Data curation. **Musolino Vincenzo:** Writing – review & editing, Writing – original draft, Visualization, Supervision, Investigation, Formal analysis, Data curation, Conceptualization.

Declaration of Competing Interest

The authors declare that they have no known competing financial

interests or personal relationships that could have appeared to influence the work reported in this paper.

Data Availability

Data will be made available on request.

Acknowledgements

We thank Prof. Massimo Borelli (UMG School of PhD Programmes, University "Magna Graecia", Catanzaro, Italy) and Prof. Lucio Torelli (Department of Medical, Surgical and Health Sciences, University of Trieste, Italy) for supervising statistical analysis.

Appendix A. Supporting information

Supplementary data associated with this article can be found in the online version at doi:10.1016/j.phrs.2024.107087.

References

[1] F. Pinna, F. Suprani, V. Deiana, L. Lai, M. Manchia, P. Paribello, G. Somaini, E. Diana, E.F. Nicotra, F. Farci, M. Ghiani, R. Cau, M. Tuveri, E. Cossu, E. Loy, A. Crapanzano, P. Grassi, A. Loviselli, F. Velluzzi, B. Carpiniello, Depression in diabetic patients: what is the link with eating disorders? Results of a study in a representative sample of patients with type 1 diabetes, Front. Psychiatry 13 (2022) 848031.
[2] R.C. Kessler, The costs of depression, Psychiatr. Clin. North Am. 35 (2012) 1–14.
[3] F. Pinna, C. Sardu, W. Orrù, F. Velluzzi, A. Loviselli, P. Contu, et al., Psychopathology, psychosocial factors and obesity, Riv. Psichiatr. 51 (2016) 30–36.
[4] B. Carpiniello, F. Pinna, G. Pillai, V. Nonnoi, E. Pisano, S. Corrias, et al., Psychiatric comorbidity and quality of life in obese patients. results from a case-control study, Int J. Psychiatry Med 39 (2009) 63–78.
[5] B. Carpiniello, F. Pinna, G. Pillai, V. Nonnoi, E. Pisano, S. Corrias, et al., Obesity and psychopathology. A study of psychiatric comorbidity among patients attending a specialist obesity unit, Epidemiol. Psichiatr Soc. 18 (2009) 119–127.
[6] B. Carpiniello, F. Pinna, R. Pili, F. Velluzzi, A. Loviselli, Mental disorders in obese patients with and without metabolic syndrome, Int J. Psychiatry Med 42 (2011) 369–375.
[7] B. Carpiniello, F. Pinna, F. Velluzzi, A. Loviselli, Mental disorders in patients with metabolic syndrome. The key role of central obesity, Eat. Weight Disord. 17 (2012) e259–e266.
[8] C.D. Moulton, J.C. Pickup, K. Ismail, The link between depression and diabetes: the search for shared mechanisms, Lancet Diabetes Endocrinol. 3 (6) (2015) 461–471.
[9] S.V. Bădescu, C. Tătaru, L. Kobylinska, E.L. Georgescu, D.M. Zahiu, A.M. Zăgrean, L. Zăgrean, The association between Diabetes mellitus and depression, J. Med. life 9 (2) (2016) 120–125.
[10] F. Pinna, F. Suprani, V. Deiana, L. Lai, M. Manchia, P. Paribello, G. Somaini, E. Diana, E.F. Nicotra, F. Farci, M. Ghiani, R. Cau, M. Tuveri, E. Cossu, E. Loy, A. Crapanzano, P. Grassi, A. Loviselli, F. Velluzzi, B. Carpiniello, Depression in diabetic patients: what is the link with eating disorders? Results of a study in a representative sample of patients with type 1 diabetes, Front. Psychiatry 13 (2022) 848031.
[11] C. Crump, J. Sundquist, M.A. Winkleby, K. Sundquist, Stress resilience and subsequent risk of type 2 diabetes in 1.5 million young men, Diabetologia 59 (4) (2016) 728–733.
[12] K. Sharif, A. Watad, L. Coplan, H. Amital, Y. Shoenfeld, A. Afek, Psychological stress and type 1 diabetes mellitus: what is the link? Expert Rev. Clin. Immunol. 14 (12) (2018) 1081–1088.
[13] D.J. Korczak, S. Pereira, K. Koulajian, A. Matejcek, A. Giacca, Type 1 diabetes mellitus and major depressive disorder: evidence for a biological link, Diabetologia 54 (10) (2011) 2483–2493.
[14] P. Gilsanz, A.J. Karter, M.S. Beeri, C.P. Quesenberry Jr, R.A. Whitmer, The bidirectional association between depression and severe hypoglycemic and hyperglycemic events in type 1 diabetes, Diabetes Care 41 (3) (2018) 446–452, https://doi.org/10.2337/dc17-1566. Epub 2017 Dec 18.
[15] A. Jung, Y. Du, J. Nübel, M.A. Busch, C. Heidemann, C. Scheidt-Nave, J. Baumert, Are depressive symptoms associated with quality of care in diabetes? Findings from a nationwide population-based study, BMJ Open Diabetes Res. care 9 (1) (2021) e001804.
[16] K. Kozieł, E.M. Urbanska, Kynurenine pathway in diabetes mellitus-novel pharmacological target? Cells 12 (3) (2023) 460.
[17] E.R. Paul, L. Schwieler, S. Erhardt, S. Boda, A. Trepci, R. Kämpe, A. Asratian, L. Holm, A. Yngve, R. Dantzer, et al., Peripheral and central kynurenine pathway abnormalities in major depression, Brain Behav. Immun. 101 (2022) 136–145.
[18] M.I. Butler, C. Long-Smith, G.M. Moloney, S. Morkl, S.M. O'Mahony, J.F. Cryan, G. Clarke, T.G. Dinan, The immune-kynurenine pathway in social anxiety disorder, Brain Behav. Immun. 99 (2021) 317–326.
[19] G. Oxenkrug, M. van der Hart, J. Roeser, P. Summergrad, Anthranilic acid: a potential biomarker and treatment target for schizophrenia, Ann. Psychiatry Ment. Health 4 (2016) 1059.
[20] G. Oxenkrug, M. van der Hart, J. Roeser, P. Summergrad, Peripheral kynurenine-3-monooxygenase deficiency as a potential risk factor for metabolic syndrome in schizophrenia patients, Integr. Clin. Med. 1 (2017).
[21] B. Li, W. Yang, T. Ge, Y. Wang, R. Cui, Stress induced microglial activation contributes to depression, Pharmacol. Res. 179 (2022) 106145.
[22] A. Muneer, Kynurenine pathway of tryptophan metabolism in neuropsychiatric disorders: pathophysiologic and therapeutic considerations, Clin. Psychopharmacol. Neurosci.: Off. Sci. J. Korean Coll. Neuropsychopharmacol. 18 (4) (2020) 507–526.
[23] J.J. Maller, et al., Increased hippocampal tail volume predicts depression status and remission to anti-depressant medications in major depression, Mol. Psychiatry 23 (2018) 1737–1744.
[24] K.M. Han, et al., Hippocampal subfield volumes in major depressive disorder and bipolar disorder, Eur. Psychiatry 57 (2019) 70–77.
[25] A. Surget, C. Belzung, Adult hippocampal neurogenesis shapes adaptation and improves stress response: a mechanistic and integrative perspective, Mol. Psychiatry 27 (2022) 403–421.
[26] S.S. Schwartz, et al., The time is right for a new classification system for diabetes: rationale and implications of the β-cell-centric classification schema, Diabetes Care 39 (2016) 179–186.
[27] K.W. Sühs, et al., Kynurenine Is a Cerebrospinal Fluid Biomarker for Bacterial and Viral Central Nervous System Infections, J. Infect. Dis. 220 (2019) 127–138.
[28] L. Mouchiroud, et al., The NAD(+)/sirtuin pathway modulates longevity through activation of mitochondrial UPR and FOXO signaling, Cell 154 (2013) 430–441.
[29] E.M. Gál, A.D. Sherman, L-kynurenine: its synthesis and possible regulatory function in brain, Neurochem. Res. 5 (1980) 223–239.
[30] F. Joubert, et al., CK flux or direct ATP transfer: versatility of energy transfer pathways evidenced by NMR in the perfused heart, Mol. Cell Biochem 256-257 (2004) 43–58.
[31] F. Joubert, J.L. Mazet, P. Mateo, J.A. Hoerter, 31P NMR detection of subcellular creatine kinase fluxes in the perfused rat heart: contractility modifies energy transfer pathways, J. Biol. Chem. 277 (2002) 18469–18476.
[32] T.Y. Lipskaya, M.S. Savchenko, Once again about the functional coupling between mitochondrial creatine kinase and adenine nucleotide translocase, Biochemistry 68 (2003) 68–79.
[33] B. Chance, The Energy-linked reaction of calcium with mitochondria, J. Biol. Chem. 240 (1965) 2729–2748.
[34] L.E. Meyer, et al., Mitochondrial creatine kinase activity prevents reactive oxygen species generation: antioxidant role of mitochondrial kinase-dependent ADP re-cycling activity, J. Biol. Chem. 281 (2006) 37361–37371.
[35] S.S. Korshunov, V.P. Skulachev, A.A. Starkov, High protonic potential actuates a mechanism of production of reactive oxygen species in mitochondria, FEBS Lett. 416 (1997) 15–18.
[36] C.M. Lloyd, J.R. Lawson, P.J. Hunter, P.F. Nielsen, The CellML model repository, Bioinformatics 24 (2008) 2122–2123.
[37] A.C. Lee, M. Zizi, M. Colombini, Beta-NADH decreases the permeability of the mitochondrial outer membrane to ADP by a factor of 6, J. Biol. Chem. 269 (1994) 30974–30980.
[38] H. Hettling, J.H. van Beek, Analyzing the functional properties of the creatine kinase system with multiscale 'sloppy' modeling, PLoS Comput. Biol. 7 (2011) e1002130.
[39] H. Noack, J. Lindenau, F. Rothe, K. Asayama, G. Wolf, Differential expression of superoxide dismutase isoforms in neuronal and glial compartments in the course of excitotoxically mediated neurodegeneration: relation to oxidative and nitrergic stress, Glia 23 (1998) 285–297.
[40] R.A. Santana-Martínez, et al., The therapeutic effect of curcumin in quinolinic acid-induced neurotoxicity in rats is associated with BDNF, ERK1/2, Nrf2, and antioxidant enzymes, Antioxidants 8 (2019) 388.
[41] C. Portera-Cailliau, et al., Non-NMDA and NMDA receptor-mediated excitotoxic neuronal deaths in adult brain are morphologically distinct: further evidence for an apoptosis-necrosis continuum, J. Comp. Neurol. 378 (1997) 88–104.
[42] P.E. Hughes, T. Alexi, T. Yoshida, S.S. Schreiber, B. Knusel, Excitotoxic lesion of rat brain with quinolinic acid induces expression of p53 messenger RNA and protein and p53-inducible genes Bax and Gadd-45 in brain areas showing DNA fragmentation, Neuroscience 74 (1996) 1143–1160.
[43] Y.M. Bordelon, L. Mackenzie, M.F. Chesselet, Morphology and compartmental location of cells exhibiting DNA damage after quinolinic acid injections into rat striatum, J. Comp. Neurol. 412 (1999) 38–50.
[44] E. Pérez-Navarro, N. Gavaldà, E. Gratacòs, J. Alberch, Brain-derived neurotrophic factor prevents changes in Bcl-2 family members and caspase-3 activation induced by excitotoxicity in the striatum, J. Neurochem 92 (2005) 678–691.
[45] F. Faul, E. Erdfelder, A.-G. Lang, A. Buchner, G*Power 3: A flexible statistical power analysis program for the social, behavioral, and biomedical sciences, Behav. Res. Methods 39 (2007) 175–191.
[46] M. Nollet, A.M. Le Guisquet, C. Belzung, Models of depression: unpredictable chronic mild stress in mice, Chapter 5, Unit 5, Curr. Protoc. Pharm. (2013) 65.
[47] V. Musolino, et al., Megestrol acetate improves cardiac function in a model of cancer cachexia-induced cardiomyopathy by autophagic modulation, J. Cachexia Sarcopenia Muscle 7 (2016) 555–566.
[48] T.D. Gould, The open field test, Mood Anxiety Relat. Phenotypes Mice (2009).
[49] S. Nucera, et al., MAFLD progression contributes to altered thalamus metabolism and brain structure, Sci. Rep. 12 (2022) 1207.

[50] V. Bouwman, et al., Depression, anxiety and glucose metabolism in the general dutch population: the new Hoorn study, PLoS One 5 (2010) e9971.
[51] S.H. Golden, et al., Examining a bidirectional association between depressive symptoms and diabetes, JAMA 299 (2008) 2751–2759.
[52] J.S. Laake, et al., The association between depressive symptoms and systemic inflammation in people with type 2 diabetes: findings from the South London diabetes study, Diabetes Care 37 (2014) 2186–2192.
[53] J.M. Zanoveli, et al., Depression associated with diabetes: from pathophysiology to treatment, Curr. Diabetes Rev. 12 (2016) 165–178.
[54] B. Buchberger, et al., Symptoms of depression and anxiety in youth with type 1 diabetes: a systematic review and meta-analysis, Psychoneuroendocrinology 70 (2016) 70–84.
[55] M. Grey, R. Whittemore, W. Tamborlane, Depression in type 1 diabetes in children: natural history and correlates, J. Psychosom. Res. 53 (2002) 907–911.
[56] E. Buoso, F. Biundo, A. Attanzio, New therapeutic approaches against inflammation and oxidative stress in neurodegeneration, Oxid. Med. Cell. Longev. 2022 (2022) 9824350.
[57] M. Gliozzi, et al., Cholesterol homeostasis: researching a dialogue between the brain and peripheral tissues, Pharm. Res 163 (2021) 105215.
[58] J.R. Moffett, et al., Quinolinate as a marker for kynurenine metabolite formation and the unresolved question of NAD+ synthesis during inflammation and infection, Front. Immunol. 11 (2020) 31.
[59] E.A. Northam, F.J. Cameron, Understanding the diabetic brain: new technologies but old challenges, Diabetes 62 (2013) 341–342.
[60] E. Rojas-Gutierrez, et al., Alzheimer's disease and metabolic syndrome: a link from oxidative stress and inflammation to neurodegeneration, Synapse 71 (2017) e21990.
[61] S.A. Hamed, Brain injury with diabetes mellitus: evidence, mechanisms and treatment implications, Expert Rev. Clin. Pharm. 10 (2017) 409–428.
[62] M. Shinohara, N. Sato, Bidirectional interactions between diabetes and Alzheimer's disease, Neurochem. Int. 108 (2017) 296–302.
[63] K. Luc, A. Schramm-Luc, T.J. Guzik, T.P. Mikolajczyk, Oxidative stress and inflammatory markers in prediabetes and diabetes, J. Physiol. Pharmacol. 70 (2019).
[64] M.I. Yilmaz, et al., The effect of corrected inflammation, oxidative stress and endothelial dysfunction on fmd levels in patients with selected chronic diseases: a quasi-experimental study, Sci. Rep. 10 (2020) 9018.
[65] D. Furman, et al., Chronic inflammation in the etiology of disease across the life span, Nat. Med. 25 (2019) 1822–1832.
[66] J.M. Parrott, L. Redus, J.C. O'Connor, Kynurenine metabolic balance is disrupted in the hippocampus following peripheral lipopolysaccharide challenge, J. Neuroinflamm. 13 (2016) 124.
[67] F.J.H. Sorgdrager, P.J.W. Naudé, I.P. Kema, E.A. Nollen, P.P. Deyn, Tryptophan metabolism in inflammaging: from biomarker to therapeutic target, Front. Immunol. 10 (2019) 2565.
[68] R. Schwarcz, J.P. Bruno, P.J. Muchowski, H.Q. Wu, Kynurenines in the mammalian brain: when physiology meets pathology, Nat. Rev. Neurosci. 13 (2012) 465–477.
[69] J. Lier, W.J. Streit, I. Bechmann, Beyond activation: characterizing microglial functional phenotypes, Cells 10 (9) (2021) 2236.
[70] R. Castro-Portuguez, G.L. Sutphin, Kynurenine pathway, NAD+ synthesis, and mitochondrial function: Targeting tryptophan metabolism to promote longevity and healthspan, Exp. Gerontol. 132 (2020) 110841.
[71] V. Pérez-De La Cruz, P. Carrillo-Mora, A. Santamaría, Quinolinic Acid, an endogenous molecule combining excitotoxicity, oxidative stress and other toxic mechanisms, Int. J. Tryptophan Res. 5 (2012) 1–8.
[72] C. Yan, et al., Dysfunction of the neurovascular unit in diabetes-related neurodegeneration, Biomed. Pharmacother. 131 (2020) 110656.
[73] E.S. Coleman, J.C. Dennis, T.D. Braden, R.L. Judd, P. Posner, Insulin treatment prevents diabetes-induced alterations in astrocyte glutamate uptake and GFAP content in rats at 4 and 8 weeks of diabetes duration, Brain Res. 1306 (2010) 131–141.
[74] A. Kamal, G.J. Biessels, S.E. Duis, W.H. Gispen, Learning and hippocampal synaptic plasticity in streptozotocin-diabetic rats: interaction of diabetes and ageing, Diabetologia 43 (2000) 500–506.
[75] M.A. McCall, et al., Targeted deletion in astrocyte intermediate filament (Gfap) alters neuronal physiology, Proc. Natl. Acad. Sci. USA 93 (1996) 6361–6366.
[76] J.F. Clark, et al., N-acetylaspartate as a reservoir for glutamate, Med Hypotheses 67 (2006) 506–512.
[77] T. Nguyen, et al., Uncovering the Role of N-Acetyl-Aspartyl-Glutamate as a Glutamate Reservoir in Cancer, Cell Rep. 27 (2019) 491–501.e6.
[78] P. Hnilicová, et al., Current methods of magnetic resonance for noninvasive assessment of molecular aspects of pathoetiology in multiple sclerosis, Int. J. Mol. Sci. 21 (2020) 6117.
[79] R. Lugo-Huitrón, et al., Quinolinic acid: an endogenous neurotoxin with multiple targets, Oxid. Med. Cell. Longev. 2013 (2013) 104024.
[80] R.G. Tavares, et al., Quinolinic acid inhibits glutamate uptake into synaptic vesicles from rat brain, Neuroreport 11 (2000) 249–253.
[81] R.G. Tavares, et al., Quinolinic acid stimulates synaptosomal glutamate release and inhibits glutamate uptake into astrocytes, Neurochem. Int. 40 (2002) 621–627.
[82] M. Wyss, R. Kaddurah-Daouk, Creatine and creatinine metabolism, Physiol. Rev. 80 (2000) 1107–1213.
[83] T. Wallimann, et al., Creatine kinase: an enzyme with a central role in cellular energy metabolism, MAGMA 6 (1998) 116–119.
[84] V. Shoshan-Barmatz, N. Keinan, H. Zaid, Uncovering the role of VDAC in the regulation of cell life and death, J. Bioenerg. Biomembr. 40 (2008) 183–191.
[85] V. Shoshan-Barmatz, E.N. Maldonado, Y. Krelin, VDAC1 at the crossroads of cell metabolism, apoptosis and cell stress, Cell Stress 1 (2017) 11–36.
[86] A. Magrì, S.A.M. Cubisino, G. Battiato, C.L.R. Lipari, S. Conti Nibali, M.W. Saab, A. Pittalà, et al., VDAC1 knockout affects mitochondrial oxygen consumption triggering a rearrangement of ETC by impacting on complex i activity, Int. J. Mol. Sci. 24 (4) (2023) 3687.
[87] A.B. Lehr, A. Kumar, C. Tetzlaff, T. Hafting, M. Fyhn, T.M. Stöber, CA2 beyond social memory: Evidence for a fundamental role in hippocampal information processing, Neurosci. Biobehav. Rev. 126 (2021) 398–412.
[88] A. Verkhratsky, A. Butt, B. Li, P. Illes, R. Zorec, A. Semyanov, Y. Tang, M. V. Sofroniew, Astrocytes in human central nervous system diseases: a frontier for new therapies, Signal Transduct. Target. Ther. 8 (1) (2023) 396.
[89] A. Popov, A. Brazhe, P. Denisov, O. Sutyagina, L. Li, N. Lazareva, A. Verkhratsky, A. Semyanov, Astrocyte dystrophy in ageing brain parallels impaired synaptic plasticity, Aging Cell 20 (3) (2021) e13334.
[90] E. Coleman, R. Judd, L. Hoe, J. Dennis, P. Posner, Effects of diabetes mellitus on astrocyte GFAP and glutamate transporters in the CNS, Glia 48 (2) (2004) 166–178.
[91] R. Troubat, et al., Neuroinflammation and depression: a review, Eur. J. Neurosci. 53 (2021) 151–171.
[92] D.W. O'Connor, D. Ames, B. Gardner, M. King, Psychosocial treatments of behavior symptoms in dementia: a systematic review of reports meeting quality standards, Int. Psychogeriatr. 21 (2009) 225–240.
[93] C. Belzung, Innovative drugs to treat depression: did animal models fail to be predictive or did clinical trials fail to detect effects, Neuropsychopharmacology 39 (2014) 1041–1051.
[94] C.M. Díaz-García, et al., Neuronal stimulation triggers neuronal glycolysis and not lactate uptake, 361-374.e4, Cell Metab. 26 (2017), 361-374.e4.
[95] H.D. Schmidt, R.S. Duman, The role of neurotrophic factors in adult hippocampal neurogenesis, antidepressant treatments and animal models of depressive-like behavior, Behav. Pharmacol. 18 (2007) 391–418.
[96] S. Naskar, S. Chattarji, Stress elicits contrasting effects on the structure and number of astrocytes in the Amygdala versus Hippocampus. *eNeuro*, *6*(1), ENEURO (2019), 0338-18.2019.
[97] L. Saur, P.P. Baptista, P.B. Bagatini, L.T. Neves, R.M. de Oliveira, S.P. Vaz, K. Ferreira, S.A. Machado, R.G. Mestriner, L.L. Xavier, Experimental post-traumatic stress disorder decreases astrocyte density and changes astrocytic polarity in the CA1 hippocampus of male rats, Neurochem. Res. 41 (4) (2016) 892–904.
[98] Z. Chen, Z. Yuan, S. Yang, Y. Zhu, M. Xue, J. Zhang, L. Leng, Brain Energy Metabolism: Astrocytes in Neurodegenerative Diseases, CNS Neurosci. Ther. 29 (1) (2023) 24–36.
[99] G. Bonvento, J.P. Bolaños, Astrocyte-neuron metabolic cooperation shapes brain activity, Cell Metab. 33 (8) (2021) 1546–1564.
[100] P. Pacher, J.S. Beckman, L. Liaudet, Nitric oxide and peroxynitrite in health and disease, Physiol. Rev. 87 (1) (2007) 315–424.
[101] A. Almeida, J. Almeida, J.P. Bolaños, S. Moncada, Different responses of astrocytes and neurons to nitric oxide: the role of glycolytically generated ATP in astrocyte protection, Proc. Natl. Acad. Sci. USA 98 (26) (2001) 15294–15299.
[102] L.A. Voloboueva, S.W. Suh, R.A. Swanson, R.G. Giffard, Inhibition of mitochondrial function in astrocytes: implications for neuroprotection, J. Neurochem. 102 (4) (2007) 1383–1394.
[103] A. San Martín, R. Arce-Molina, A. Galaz, G. Pérez-Guerra, L.F. Barros, Nanomolar nitric oxide concentrations quickly and reversibly modulate astrocytic energy metabolism, J. Biol. Chem. 292 (22) (2017) 9432–9438.
[104] A. Almeida, S. Moncada, J.P. Bolaños, Nitric oxide switches on glycolysis through the AMP protein kinase and 6-phosphofructo-2-kinase pathway, Nat. Cell Biol. 6 (1) (2004) 45–51.
[105] S. Kim, Y. Son, Astrocytes stimulate microglial proliferation and M2 polarization in vitro through crosstalk between astrocytes and microglia, Int. J. Mol. Sci. 22 (16) (2021) 8800.
[106] M.R. Abbink, A.F. van Deijk, V.M. Heine, M.H. Verheijen, A. Korosi, The involvement of astrocytes in early-life adversity induced programming of the brain, Glia 67 (9) (2019) 1637–1653.
[107] Y. Zhao, Q. Zhang, X. Shao, L. Ouyang, X. Wang, K. Zhu, L. Chen, Decreased glycogen content might contribute to chronic stress-induced atrophy of hippocampal astrocyte volume and depression-like behavior in rats, Sci. Rep. 7 (2017) 43192.
[108] W. Li, G. Roy Choudhury, A. Winters, J. Prah, W. Lin, R. Liu, S.H. Yang, Hyperglycemia alters astrocyte metabolism and inhibits astrocyte proliferation, Aging Dis. 9 (4) (2018) 674–684.
[109] Y. Zhu, et al., Cardiac PI3K-Akt impairs insulin-stimulated glucose uptake independent of mTORC1 and GLUT4 translocation, Mol. Endocrinol. 27 (2013) 172–184.
[110] J.H. Xie, Y.Y. Li, J. Jin, The essential functions of mitochondrial dynamics in immune cells, Cell Mol. Immunol. 17 (2020) 712–721.
[111] X.L. Wang, S.T. Feng, Z.Z. Wang, N.H. Chen, Y. Zhang, Role of mitophagy in mitochondrial quality control: Mechanisms and potential implications for neurodegenerative diseases, Pharmacol. Res. 165 (2021) 105433.
[112] M. Tang, T. Liu, P. Jiang, R. Dang, The interaction between autophagy and neuroinflammation in major depressive disorder: From pathophysiology to therapeutic implications, Pharmacol. Res. 168 (2021) 105586.

[113] H.Q. Wang, Z.Z. Wang, N.H. Chen, The receptor hypothesis and the pathogenesis of depression: Genetic bases and biological correlates, Pharmacol. Res. 167 (2021) 105542.
[114] J.L. Warner-Schmidt, R.S. Duman, VEGF is an essential mediator of the neurogenic and behavioral actions of antidepressants, Proc. Natl. Acad. Sci. USA 104 (2007) 4647–4652.
[115] T. Strekalova, et al., Hippocampal over-expression of cyclooxygenase-2 (COX-2) is associated with susceptibility to stress-induced anhedonia in mice, Int. J. Mol. Sci. 23 (2022) 2061.
[116] Y. Takayanagi, et al., Hippocampal volume reduction correlates with apathy in traumatic brain injury, but not schizophrenia, J. Neuropsychiatry Clin. Neurosci. 25 (2013) 292–301.
[117] W.B. Kim, J.H. Cho, Encoding of contextual fear memory in hippocampal-amygdala circuit, Nat. Commun. 11 (2020) 1382.
[118] V. Castagné, et al., Behavioral Assessment of Antidepressant Activity in Rodents, in: J.J. Buccafusco (Ed.), Methods of Behavior Analysis in Neuroscience, 2nd ed., CRC Press/Taylor & Francis, 2009.
[119] A. Du Preez, et al., Chronic stress followed by social isolation promotes depressive-like behaviour, alters microglial and astrocyte biology and reduces hippocampal neurogenesis in male mice, Brain Behav. Immun. 91 (2021) 24–47.
[120] M. Becker, A. Pinhasov, A. Ornoy, Animal models of depression: what can they teach us about the human disease, Diagnostics 11 (2021) 123.
[121] F. Cathomas, M.N. Hartmann, E. Seifritz, C.R. Pryce, S. Kaiser, The translational study of apathy-an ecological approach, Front Behav. Neurosci. 9 (2015) 241.
[122] A. Ennaceur, P.L. Chazot, Preclinical animal anxiety research - flaws and prejudices, Pharm. Res Perspect. 4 (2016) e00223.
[123] Kim, E.J. & Kim, J.J. Neurocognitive effects of stress: a metaparadigm perspective. *Mol Psychiatry* 10.1038/s41380–023-01986–4.
[124] M.A. Bayani, A. Talebnia Roshan, S. Moudi, H. Gholinia Ahangar, Sertraline and fluoxetine in adult patients with comorbid depression and type ii diabetes mellitus: a randomized controlled trial, Jundishapur J. Chronic Dis. Care 13 (1) (2024) e138454.